https://doi.org/10.5194/egusphere-2026-4156
Preprint. Discussion started: 2 September 2026

Deriving Precipitation and Latent Heating Profiles from NASA TROPICS Smallsat through a Two-Step Ensemble Convolution Neural Network Method

Toshi Matsui[1&2], Scott A. Braun[1], Sarah E. Ringerud[1]

[1]Mesoscale Atmospheric Processes Laboratory, NASA Goddard Space Flight Center, Greenbelt, MD, USA
[2]Earth System Science Interdisciplinary Center – ESSIC, University of Maryland, College Park, MD, USA

Submitted to EGU Atmospheric Measurement Techniques (AMT)

Corresponding Authors:
Toshi Matsui, Toshihisa.Matsui-1@nasa.gov
ESSIC UMD
Code 612, NASA Goddard Space Flight Center
Greenbelt, 21617, MD, USA

https://doi.org/10.5194/egusphere-2026-4156
Preprint. Discussion started: 2 September 2026

Abstract: This study develops and implements a two-step ensemble convolutional neural network (CNN) framework to retrieve precipitation and latent heating (LH) profiles from passive-microwave observations from NASA's Time-Resolved Observations of Precipitation structure and storm Intensity with a Constellation of Smallsats (TROPICS) mission. In the first step, a precipitation CNN is trained using collocated TROPICS brightness temperatures (Tb) and Global Precipitation Measurement (GPM) combined radar-radiometer (2BCMB) precipitation estimates. Ensemble CNN training shows that retrieval skill is controlled by interactions among a set of choices for hyperparameters, including optimizer settings, architecture depth, and loss weighting. Orbital-scale global evaluation is also required for final model selection because precipitation-intensity distributions differ across tropical environments. Relative to the baseline TROPICS Precipitation Retrieval and Profiling Scheme (PRPS), the CNN retrieval reproduces the large-scale climatological structure of GPM precipitation more accurately in terms of correlations and biases. The CNN produces greater frequencies of heavier precipitation than PRPS; however, the heaviest precipitation frequencies remain underrepresented in the CNN due to the limited number of training samples. In the second step, the same TROPICS Tb patches are used to retrieve GPM Convective–Stratiform Heating (CSH) LH profiles from 1 to 12 km altitude, while the first-step CNN precipitation retrieval provides an additional physical constraint through a precipitation–LH budget linkage. The resulting LH climatology compares favorably with GPM CSH products in both horizontal maps and zonal vertical structure. The CNN reproduces the broad tropical heating maxima, their mid-tropospheric placement, and their meridional extent over land and ocean, with the best agreement generally occurring in the 5-7.5 km layer. These results demonstrate that, despite limited single-footprint information content, a two-step ensemble CNN framework can retrieve physically realistic precipitation and LH structure from TROPICS observations.

Short Summary: This study shows how NASA's TROPICS small satellites can estimate tropical rainfall and latent heating using a deep-learning method trained with GPM satellite data. The spatial texture of microwave observations from space provides useful information for producing realistic views of rainfall and storm-heating structure across the Tropics.

https://doi.org/10.5194/egusphere-2026-4156
Preprint. Discussion started: 2 September 2026

Introduction

Understanding the organization and evolution of tropical convection remains a central challenge in atmospheric science and Earth-system modeling. Convective processes redistribute energy vertically and laterally, thereby playing a key role in modulating the large-scale circulation and energy and water cycles (Gill, 1980; Houze, 1982; Mapes, 2001). Key components that govern this redistribution include latent heating (LH) from condensation/deposition, evaporation/sublimation, and freezing/melting of water, and radiative heating due to solar heating and infrared emission from Earth (Hartmann et al., 1984; Stephens et al., 2012). Latent heating associated with deep convection is a major driver of general circulation in the Tropics and contributes to the generation and maintenance of mesoscale convective systems and tropical cyclones (Riehl and Malkus, 1958; Webster, 1972; Schumacher et al., 2004; Hagos and Zhang, 2010). Radiative cooling (primarily longwave) balances convective heating and modulates cloud-radiation feedback (e.g., Chou and Neelin, 2004). A complete understanding of tropical energy exchange processes, therefore, requires accurate and collocated estimates of both latent and radiative energy sources (Matsui et al., 2015; Chen et al., 2025).

While radiative heating has been well constrained by the Clouds and the Earth's Radiant Energy System (CERES) and combined geostationary satellites (Wielicki et al., 1996; Loeb et al., 2016), the observational constraints on LH remain limited due to the complexity of its vertical structure and dependence on cloud microphysical processes (Chen et al., 2025). Retrievals from the Tropical Rainfall Measuring Mission (TRMM) and the Global Precipitation Measurement (GPM) Core Observatory have enabled significant progress (e.g., Tao et al., 2022), but revisit times have been limited by the poor sampling from single satellite observations. In addition, current LH retrieval studies have focused on using either or both radar and passive microwave radiometer measurements; the algorithms only utilize single pixel/profile information, and their coupled temporal evolution remains poorly constrained observationally (Tao et al., 1993; Shige et al., 2004; Grecu et al., 2009; Yang and Smith, 1999; Satoh and Noda, 2001). The Time-Resolved Observations of Precipitation structure and storm Intensity with a Constellation of Smallsats (TROPICS) mission with its constellation of smallsats in low-inclination orbits and ~1-hour median revisit rate, presents a transformative opportunity to track the time-evolving vertical structure of tropical convection at high cadence (Blackwell et al., 2018, 2025); however, these

https://doi.org/10.5194/egusphere-2026-4156
Preprint. Discussion started: 2 September 2026

smallsats have limited information to estimate LH from the course-resolution high-frequency passive microwave observations.

The recent evolution of deep neural networks, especially the Convolution Neural Network (CNN) approach, for satellite retrievals moves from pixel-wise, shallow neural-network methods that treat each observation independently to deeper, spatially aware, and probabilistic frameworks that exploit the image-like structure of satellite footprint arrays. Early neural-network (NN)-based precipitation retrievals from passive microwave observations are largely developed as single-footprint methods (e.g., Staelin and Chen, 2000; Surussavadee and Staelin, 2008; Sanò et al., 2018; Tang et al., 2018), which limit their ability to exploit the mesoscale organization of precipitating systems. More recent studies show that CNNs can use surrounding scene structure more effectively, including for infrared-based retrievals (Sadeghi et al., 2019) and passive-microwave precipitation detection (Li et al., 2021). For passive-microwave retrievals, Pfreundschuh et al. (2022) replace the operational Goddard Profiling (GPROF) algorithm with a CNN approach, which improves retrieval accuracy while preserving operational compatibility. Afzali Gorooh et al. (2023) further demonstrate that optimal satellite precipitation retrieval increasingly depends on the synergistic use of lower-orbiting passive-microwave and geostationary-satellite observations rather than on either data source alone. In parallel, Gavahi et al. (2023) show that CNN-based methods can also be extended from direct retrieval to multisource precipitation fusion, using a hybrid deep neural network framework to merge and downscale multiple satellite, gauge, and reanalysis products while explicitly exploiting spatiotemporal dependencies. An additional recent advancement is the development of near-real-time multi-satellite retrieval systems that ingest raw Level-1 geostationary and passive-microwave observations in a sequence-based CNN framework rather than relying on morphed microwave precipitation inputs (Cannon et al., 2026). Together, these studies indicate that the most important recent advances in CNN-based precipitation estimation are the use of spatial context, probabilistic prediction, direct ingestion of heterogeneous Level-1 observations, and flexible multi-sensor fusion, all of which are improving the realism and utility of satellite precipitation retrievals.

This manuscript further takes advantage of the range of microwave frequencies available with the TROPICS sounder for sensing the vertical profile of LH through a novel two-step ensemble CNN

https://doi.org/10.5194/egusphere-2026-4156
Preprint. Discussion started: 2 September 2026

framework using data from GPM-based LH products as training targets. Although the information available within a single TROPICS footprint is limited for characterizing precipitation systems compared with dedicated precipitation missions (e.g., Kidd et al., 2021a), the spatial structure of brightness temperature fields provide valuable information for vertical atmospheric profiling, as previously demonstrated in temperature and humidity retrieval studies (Yang et al., 2023). Section 2 of this study describes the TROPICS satellites, the GPM LH products, and the methodology for the two-step ensemble CNN training and subsequent precipitation and LH retrievals. Section 3 presents the CNN ensemble training results and the validation of the precipitation and LH retrievals through comparisons with base GPM LH satellite products. Further investigation will also reveal the importance of Tb patches and channels for retrievals. Section 4 summarizes the main findings, discusses their implications, and outlines future directions. Note that instantaneous validation against ground-based measurements is beyond the scope of this manuscript. Such validation will be conducted once retrievals from the full TROPICS constellation become available in the near future.

1. Data and Method

2.1 GPM Combined Precipitation and Latent Heating Products

The Goddard Convective–Stratiform Heating (CSH) algorithm is a process-model-informed LH retrieval developed for TRMM and GPM to estimate the vertical structure of diabatic heating associated with precipitating cloud systems (Tao et al., 2022). Because LH (water phase changes) cannot be measured directly by satellite or in-situ observations, the CSH method uses lookup tables (LUTs) derived from cloud-resolving model (CRM) simulations to relate observed precipitation characteristics to representative heating profiles (Tao et al., 1993, 2010). In the GPM framework, the retrieval uses the Combined radar–radiometer product (2BCMB; Grecu et al., 2016; Olson, W. S. and the GPM Combined Radar-Radiometer Algorithm Team, 2022) as input, including surface rain rate, convective/stratiform classification, and echo-top height extending from the Tropics to midlatitude regions (Lang and Tao, 2018; Tao et al., 2019).

https://doi.org/10.5194/egusphere-2026-4156
Preprint. Discussion started: 2 September 2026

In the current GPM version (V7), CSH is built around the physically distinct heating structures of convective and stratiform precipitation, with separate LUTs binned by rain-rate intensity, precipitation type, echo-top height, and low-level reflectivity gradient, and with different LUTs over land and ocean (Tao et al., 2022). The primary product is the Level-2 pixel retrieval (2HCSH) (Tao and Lang, 2016). A major strength of the approach is that it reproduces the canonical vertical heating signatures of net heating in convective regions and heating aloft over cooling below in stratiform regions, and its vertically integrated heating is broadly consistent with the GPM 2BCMB rainfall, especially over the ocean and in the Intertropical Convergence Zone (ITCZ) region (Tao et al., 2022). On the other hand, the main weakness of CSH, and other satellite LH retrievals more generally, is that the product is not a direct observation but an inferred quantity that depends on both the precipitation input and the representativeness of the model-derived LUTs (Tao et al., 2022). The retrieved heating magnitude is sensitive to 2BCMB rain rates, while the vertical structure is sensitive to the convective–stratiform partitioning and to the limited set of CRM cases used to construct the LUTs (Tao and Lang, 2016). As a result, agreement is generally better over the ocean than over land, local differences can be substantial at 0.25° resolution, and the equivalent rain-rate distributions tend to show too much light rain and too little heavy rain relative to the 2BCMB product (Tao et al., 2022). Thus, CSH should be best interpreted as a physically constrained diagnostic product for regional-to-large-scale heating structure and climatology, rather than a precise instantaneous, event-scale dataset (Tao et al., 2022).

As mentioned in the introduction, the CSH methodology depends critically on vertical precipitation information from the narrow-swath single-satellite GPM combined radar–radiometer product, which severely limits global coverage and revisit frequency, leaving large temporal gaps during rapidly evolving convection. These sampling and structural limitations highlight the need for complementary approaches of using frequent-visiting microwave radiometer observations to provide more continuous LH information across the Tropics and improve our understanding of convective energetics. The CSH V7 retrieval is also limited to terrain below 1000 m.

2.2 TROPICS SmallSat Mission

The TROPICS mission was developed to address a long-standing observational limitation in tropical cyclone monitoring, namely the sparse temporal sampling of passive microwave

https://doi.org/10.5194/egusphere-2026-4156
Preprint. Discussion started: 2 September 2026

measurements over tropical latitudes. In contrast to conventional high-inclination microwave missions, TROPICS employed a low-inclination CubeSat constellation designed to provide substantially improved revisit times over the Tropics, thereby enabling more continuous observations of rapidly evolving storm structures and their surrounding environments. The satellites carried a 12-channel cross-track-sampling microwave radiometer, including temperature-sensitive channels near the 118.75-GHz O_2 line, water-vapor channels around 183.31 GHz, and high-frequency window and ice-scattering channels near 91.655 GHz and 204.8 GHz. Nadir footprint sizes were 30 km for the 91.655 GHz channel, 24 km for the 114.5~118.58 GHz channels, 17 km for the 184.41~190.31GHz channels, and 15 km for the 204.8 GHz channel, and these footprints became larger off the nadir positions (Blackwell et al., 2025). Therefore, the radiometers observed key thermodynamic and hydrometeor-related signals associated with deep convection, precipitation, and tropospheric moisture. This observing strategy was particularly valuable for tropical cyclone applications because passive microwave measurements can reveal storm structure beneath upper-level cloud canopies that are not directly observed by visible and infrared imagery alone (Blackwell et al., 2018, 2025).

The TROPICS data record includes both Level-1 (L1) radiance products and Level-2 (L2) geophysical retrieval products. The radiometric calibration of L1b brightness temperatures (Tb) is generally stable in time, with departures from simulated radiances typically less than about 1 K for most channels, supporting the use of these observations for L2 retrieval development and other quantitative applications (Blackwell et al., 2025). TROPICS L2 products include atmospheric vertical temperature and moisture profiles (Yang et al., 2023), instantaneous surface rain rate (Kidd et al., 2022), and tropical-cyclone intensity products.

The Precipitation Retrieval and Profiling Scheme (PRPS, Kidd et al., 2022) matches TROPICS L1 observations to GPM GMI precipitation estimates to derive precipitation from each TROPICS sensor. The PRPS retrievals already satisfy the TROPICS mission requirement of agreement within 25% of the GPM IMERG product at the target scale. At the instantaneous scale, comparisons with Multi-Radar, Multi-Sensor (MRMS) rain rates over the United States show that PRPS reproduces the main precipitation extent and intensity reasonably well in terms of mean errors and correlation coefficients (Kidd et al., 2022). On the other hand, single-footprint retrieval accuracy remains limited by 1) ambiguity between ice and rain signals, 2) surface-emissivity effects, and 3) reduced sensitivity to heavy precipitation due to a lack of low-frequency channels (less than 34GHz) and dual polarization Tb measurements (Kidd et al., 2016, 2021b). These challenges motivate the development of a ML approach that leverages multi-frequency spatial texture in addition to the traditional single-footprint retrieval to improve precipitation and LH estimates. The TROPICS PRPS product, in addition to the GPM combined retrieval, is also used to evaluate TROPICS CNN precipitation estimates.

2.3 TROPICS Two-Step Ensemble Deep Learning Approach

This manuscript takes advantage of TROPICS's sounding capability to estimate vertical profiles of LH by fusing TROPICS L1 brightness temperatures with coincident GPM LH profiles (Tao and Lang. ATBD). For this purpose, the TROPICS precipitation-LH CNN framework operates in two sequential stages. First, a precipitation-retrieval CNN is trained using multi-frequency TROPICS brightness temperatures and coincident reference GPM combined radar-radiometer (2BCMB) precipitation, allowing the algorithm to learn robust spectral–spatial relationships associated with surface rain rate. In the second stage, the resulting precipitation estimates serve as constraints for training a LH profile retrieval, together with physically based relationships between column precipitation, LH magnitude and profile structure, and convective texture. This two-step strategy enables the LH algorithm to leverage precipitation-dependent structural information while also learning vertical heating patterns from coincident multi-channel TROPICS microwave Tbs and GPM LH profiles. By explicitly linking column precipitation and LH structure, the two-step approach provides a physically informed and computationally flexible framework for retrieving LH profiles from TROPICS observations.

The CNN development follows this framework while being adapted to the observing characteristics of the TROPICS sounders. First, GPM 2BCMB precipitation estimates, originally available at an effective footprint of about 5 km, are aggregated to the larger TROPICS sounder footprint used in this study (30 km), provided that the sampling time difference between the two observations is within 1) 15 min and 2) 30min. While 30-min matchup databases introduce larger temporal discrepancy of precipitation and Tb, it increases sampling volume to nearly twice as

https://doi.org/10.5194/egusphere-2026-4156
Preprint. Discussion started: 2 September 2026

much as 15-min matchup databases. The larger data volume is likely critical to achieving adequate representation of heavy precipitation. Here, 15-min and 30-min databases are independently trained, and we evaluate the retrieved global precipitation to determine the final best CNN models.

The CNN input consists of 7 × 7 patches of TROPICS Tb, together with auxiliary information describing the land–ocean mask and data quality. The 7 × 7 patch size is selected based on initial testing to balance the use of textural information with the number of available training samples. Larger patch sizes slow the training process, reduce the number of training samples because of greater memory requirements, and do not provide clear improvement. Verification results are presented in Section 3.3. In the present configuration, the input therefore includes 14 parameters: the 12 TROPICS channel Tb fields, a binary land–ocean mask, and quality-control information. The same Tb quality-control criteria used in the TROPICS PRPS retrieval are applied here to ensure that only physically reliable observations are used. Accordingly, samples affected by solar intrusion, lunar intrusion, spacecraft maneuvers, or hot/cold calibration periods are excluded from the training dataset (Kidd et al., 2022). Figure 1 shows a single-case example from the TROPICS–GPM match-up database, illustrating that TROPICS brightness temperatures at different channels respond uniquely to the GPM 2BCMB precipitation and GPM CSH LH profiles.

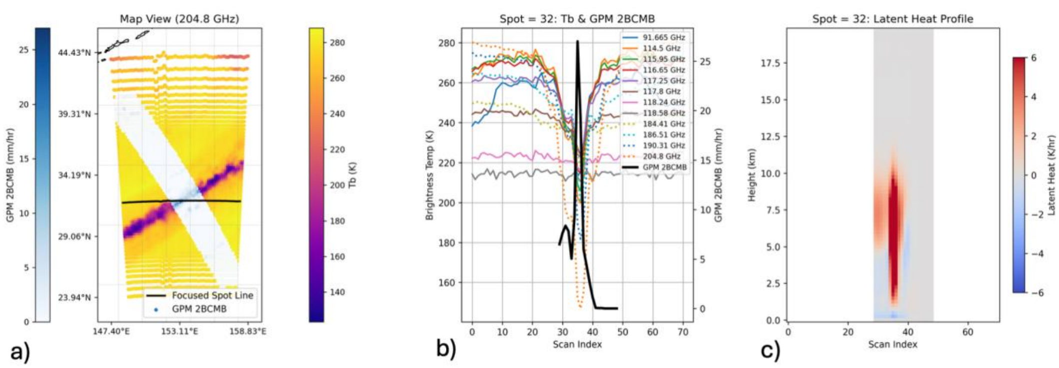

Figure 1: TROPICS Tb and GPM CSH overlapping images. a) TROPICS Tb (204.8GHz) and GPM 2BCMB precipitation with the location of vertical cross section shown. b) TROPICS Tb for all channels and GPM 2BCMB surface precipitation along the cross section. c) Vertical cross section of GPM CSH LH profiles.

https://doi.org/10.5194/egusphere-2026-4156
Preprint. Discussion started: 2 September 2026

Unlike conically scanning sensors, cross-track sensors such as TROPICS have viewing angles and footprint sizes that vary with spot (i.e., scan) position. To reduce this spot-dependent systematic variability, mean Tb climatologies are constructed for each spot position and channel, and are then used to calculate spot-normalized Tb, following the PRPS algorithm of Kidd et al. (2022). This approach is advantageous to reduce dependency of spot positions upon CNN-based training and algorithms. In addition, valid samples with sensor-maneuver angle within 0.5 degrees, finite Tb values between 50 and 350 K, and GPM CMB precipitation rates between 0 and 200 mm hr^{-1} are then used for CNN training, separately over land and ocean. These processes ensure preparation of a clean TB patch database for CNN training.

The retrieval model is a deep CNN composed of a sequence of 3 × 3 convolutional layers. Each convolutional layer is followed by batch normalization, which stabilizes mini-batch activation statistics and improves optimization, and by rectified linear unit (ReLU) activation, which introduces nonlinearity while maintaining efficient gradient propagation (Nair and Hinton, 2010; Glorot et al., 2011; Ioffe and Szegedy, 2015). Dropout is applied after the convolutional stack to reduce overfitting by randomly suppressing a fraction of activations during training, thereby improving generalization (Srivastava et al., 2014). Adaptive average pooling is then used to reduce the final feature maps to a fixed spatial size before the output layer, providing a compact summary of the learned spatial features and simplifying the mapping to the retrieved precipitation value (Lin et al., 2013). These specialized methods are common methods to improve CNN training, available in the PyTorch module (Paszke et al., 2019).

Rather than predicting precipitation directly in physical units, the model is trained using a logarithmic transformation of precipitation. This transformation reduces the strong positive skewness of precipitation and stabilizes training across the wide range from light to heavy rain. The standard configuration allows the depth of the CNN to vary between three and five convolutional layers, thereby enabling controlled testing of the role of network complexity in retrieval performance.

https://doi.org/10.5194/egusphere-2026-4156
Preprint. Discussion started: 2 September 2026

To improve performance across the full precipitation spectrum, the model is trained using a custom loss function. The total loss of CNN, $\mathcal{L}_{precip}$, combines three components: a weighted mean-square error (MSE) term, a conditional-bias penalty term, and a histogram-matching penalty term:

$$\mathcal{L}_{precip} = \mathcal{L}_{MSE}^{W} + \lambda_{bias}\mathcal{L}_{bias} + \lambda_{hist}\,\mathcal{L}_{hist} \qquad \text{(Eq. 1)}$$

The first term, $\mathcal{L}_{MSE}^{W}$, is a pointwise mean-square error (MSE), weighted with precipitation intensity, so that heavier-rain samples contribute more strongly than light-rain samples. The second term, $\mathcal{L}_{bias}$, is a fine-bin conditional-bias penalty. This term differs from the first term because it specifically penalizes systematic overestimation or underestimation within each precipitation intensity regime, even when the pointwise MSE is otherwise acceptable. The third term, $\mathcal{L}_{hist}$, is a histogram-matching penalty designed to improve agreement between the predicted and observed precipitation-frequency distributions. This term encourages the CNN not only to minimize pointwise error, but also to reproduce the overall precipitation-intensity distribution, especially the relatively rare moderate-to-heavy rain events. The second and third terms are designed specifically to address common limitations of microwave sounder precipitation retrievals (Kidd et al.2021a), namely, low bias in the bulk distribution but poor representation of extremes, and intensity-dependent errors. The hyperparameters λ_{bias} and λ_{hist} are tunable to control the relative importance of these penalties.

Because retrieval performance can depend strongly on the choice of optimization and regularization hyperparameters, the CNN training is embedded within a systematic hyperparameter-ensemble framework. Instead of relying on a single parameter configuration, a full-factorial ensemble is constructed by varying four key parameters: 1) the learning rate of the Adam optimizer that controls the step size used to update the model parameters, 2) the weight applied to the bias-penalty term (Eq. 1), 3) the CNN learning depths, and 4) the dropout rate that controls overfitting for generalization of the model. The tested values are described in Table 1. Note that three ensemble values of λ_{hist} are also tested but eventually fixed at 0.5 to avoid overfitting of the CNN model (discussed later). Thus, a total of 91 sets (3×3×3×3) of ensemble CNN training are conducted for 15-min and 30-min TROPICS-GPM matchup databases. Details of the hyperparameter values are summarized in Table 1.

https://doi.org/10.5194/egusphere-2026-4156
Preprint. Discussion started: 2 September 2026

Parameter	Feasible Ranges and Notes
Learning Rate of Adam Optimzser	1e-5: Very slow but stable, useful if network diverges 1e-4: default 3e-4: Faster training, but risks overshooting.
Loss Bias Weights (precipitation only)	0: No bias weight 0.5: default 1.0: High bias weight
Number of Layers (precipitation only)	3: Faster training, shallower 4: Default 5: Deeper features, risk of overfitting or saturation.
Dropout Rate	0.2: Moderate overfitting for shallow networks 0.3: Default 0.5: Heavy dropout, useful for deep networks with small data

Table 1. Descriptions and ranges of precipitation CNN model hyperparameters.

For each ensemble member, the dataset is randomly divided into training and validation subsets using an 80/20 split. Model optimization is performed with an adaptive stochastic-gradient method and the Adam optimizer (Kingma and Ba, 2015), and training proceeds for up to 30 trials (i.e., epoch number) separately over land and ocean. The best performing model from each run is selected according to minimum validation loss and saved separately for land and ocean conditions. Ensemble CNN training performance is then evaluated in physical precipitation units using mean-square error (MSE), mean bias (MB), and coefficient of determination (R^2), together with log-scale scatter-density plots and precipitation intensity histogram comparisons against the GPM 2BCMB precipitation target. These diagnostics are used to assess not only pointwise retrieval accuracy, but also the ability of the CNN to reproduce the observed precipitation-intensity distribution.

Note that without precipitation histogram constraints (λ_{hist} = 0.0), the CNN training appears to achieve higher point-wise validation skill, but its application to full orbital precipitation retrievals always results in a systematic wet bias relative to the original GPM 2BCMB precipitation. In other words, pointwise training/validation metrics alone can favor models that preserve relative

https://doi.org/10.5194/egusphere-2026-4156
Preprint. Discussion started: 2 September 2026

variability but do not necessarily reproduce the observed light-to-heavy precipitation frequency distributions, which is critical to reproduce a realistic global precipitation map.

Once the best precipitation CNN models are chosen separately for land and ocean, LH profiles are trained by extending the TROPICS CNN precipitation system. Similar to the precipitation CNN model, the same 7×7 Tb patches (including land–ocean mask) are used to train 80-level LH profiles from GPM CSH data. The main difference lies in the loss function and output design. Instead of predicting surface precipitation rate, the LH CNN model outputs a vertical profile through a dense prediction layer. Because initial testing shows that predicting near-surface LH and very small LH values in the upper layers is challenging and can introduce CNN errors, the LH CNN training and algorithm are limited to 1–12 km above ground level. This altitude range captures the majority of LH variability that is important for large-scale circulation (Houze, 1982). The LH CNN is trained with a composite loss function that constrains both the vertical profile structure and its consistency with the corresponding precipitation column. The total loss of the LH CNN, $\mathcal{L}_{LH}$, is written as

$$\mathcal{L}_{LH} = \mathcal{L}_{MSE}^{LH} + \lambda_{bias}^{LH}\mathcal{L}_{bias}^{LH} + \lambda_{p-LH}\,\mathcal{L}_{p-LH}, \qquad \text{(Eq. 2)}$$

where the first term $\mathcal{L}_{MSE}^{LH}$ is a MSE loss between predicted and target LH profiles, penalizing level-by-level LH mismatches. The second term, $\mathcal{L}_{bias}^{LH}$, is a column bias loss, penalizing systematic overestimation/underestimation from the column-integrated LH. The third term, $\mathcal{L}_{p-LH}$, links energy budget consistency between the retrieved LH profile to the precipitation estimated by the first-stage precipitation CNN. The hyperparameters λ_{bias}^{LH} and λ_{p-LH} are tunable to control the relative importance of the column LH bias and precipitation-LH budget constraints. Note that these two penalties are similar, but λ_{p-LH} applies to the entire column energy budget, while λ_{bias}^{LH} applies to a certain specific range of height (1~12km, discussed later).

The third penalty term can be achieved by simultaneously applying the pre-trained precipitation CNN models to predict surface rain rate (P), which is then related to the predicted column-integrated LH budget via a column energy-closure relation

$$\int \rho(z)C_pLH(z)dz \;\approx\; L_vP, \qquad \text{(Eq. 3)}$$

https://doi.org/10.5194/egusphere-2026-4156
Preprint. Discussion started: 2 September 2026

where *LH(z)* is the LH at height *z*, *ρ(z)* is the air density at height *z*, C_p is the specific heat of air at constant pressure, and *Lv* is the latent heat of vaporization. This relation generally applies to a large-scale environment over a time scale comparable to the lifetime of convection (Yanai et al., 1973), but for convenience, this relationship is instantaneously applied for each column, enforcing energy and moisture budget consistency. These penalties are used to assess both the realism of the retrieved vertical structure and its statistical agreement with the reference LH profiles.

Parameter	Feasible Ranges and Notes
Learning Rate of Adam Optimizer	1e-5: Very slow but stable, useful if network diverges 1e-4: default 3e-4: Faster training, but risks overshooting.
Column LH bias (λ_{bias}^{LH})	0.01: Weak emphasis on removing column LH bias 0.05: default 0.1: Most attention to reducing column LH bias
Precipitation-LH budget (λ_{p-LH})	0.3: Weakest precipitation-LH coupling; the LH model is driven mostly by fitting the target LH profile itself 1.0: default 3.0: Strong constraint to ensure the column-integrated LH is consistent with the surface precipitation rate
Dropout Rate	0.2: Moderate overfitting for shallow networks 0.3: Default 0.5: Heavy dropout, useful for deep networks with small data

Table 2. Descriptions and ranges of LH CNN model hyperparameters.

Similar to the precipitation CNN training, the ensemble approach is applied to the LH CNN training (Table 2). While the learning rate of the Adam optimizer and dropout rate are still used, the main difference from the precipitation CNN model is 1) λ_{bias}^{LH} and λ_{p-LH} are introduced to control the relative importance of the column LH bias and precipitation-LH budget constraints, and 2) the number of convolutional layers is kept at five, instead of 3, 4, and 5 CNN layers used in the best-performing precipitation CNN in order to choose consistent layer numbers between the

https://doi.org/10.5194/egusphere-2026-4156
Preprint. Discussion started: 2 September 2026

precipitation and the LH training. Again, total ensemble CNN training is applied to estimate the best LH CNN model. Validation diagnostics are adapted to the profile nature of the target and include overall error statistics, level-by-level coefficients of determination, and contoured frequency by altitude diagrams (CFADs) for the target and retrieved LH profiles. These diagnostics are used to assess both the realism of the retrieved vertical structure and its statistical agreement with the reference LH profiles.

2. Results

3.1 Precipitation Training Results and Estimates

The composite Z-score used in this study is designed to combine the three main validation metrics into a single standardized ranking index. For each ensemble member, MSE, MB, and R^2 are calculated and converted into standardized Z-scores using the distribution of each metric across the ensemble. The final composite score is then defined as

$$Z_{tot} = Z(R^2) - Z(MSE) - Z(|MB|), \qquad \text{(Eq. 4)}$$

where larger R^2 increases the score, while larger |MB| and MSE decreases the score. Overall, in this formulation, a higher Z_{tot} indicates a better overall balance of skill, error, and bias across the ensemble of CNN-training members.

https://doi.org/10.5194/egusphere-2026-4156
Preprint. Discussion started: 2 September 2026

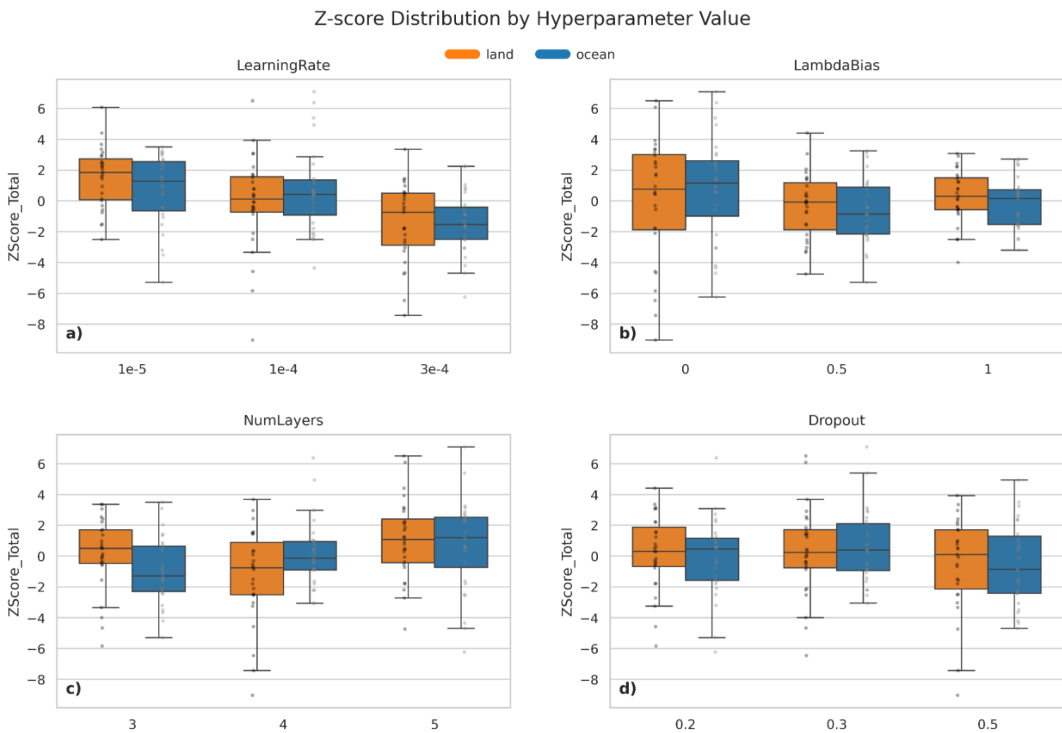

Figure 2: Box plots of Z_{tot} from each ensemble CNN-training member with respect to a) learning rate, b) lambda bias (λ_{bias}), c) the number of layers, d) dropout ratio over land and ocean. The results are from GPM-TROPICS 15-min matchup data. Gray dots show the Z_{tot} of individual ensemble members.

The spread of Z_{tot} is substantial for nearly all tested hyperparameter values over both land and ocean, but the distributions also reveal several clearer first-order tendencies than suggested by individual model results alone (Fig. 2). In all four panels, the interquartile ranges are broad, and the whiskers and outliers extend across both strongly positive and strongly negative values, indicating that no single hyperparameter by itself determines model success. Rather, the same nominal learning rate, bias-penalty weight, number of layers, or dropout value can lead to either strong or weak solutions depending on the accompanying settings. The considerable overlap among neighboring boxplots further indicates that CNN performance is governed by interactions among hyperparameter setups rather than by any one control parameter by itself. At the same time, the land and ocean distributions are broadly similar in shape, suggesting that the major sensitivities

https://doi.org/10.5194/egusphere-2026-4156
Preprint. Discussion started: 2 September 2026

are broadly shared across land and ocean, even though the optimal settings are not identical. The box plots using the match-up data within 30 minutes (not shown) are similar.

Despite the widespread in Z scores, Fig. 2 still suggests several robust tendencies. For learning rate, the smallest value (10^{-5}) yields the most favorable median Z_{tot} over both land and ocean, whereas a value of 3×10^{-4} shifts the distributions clearly downward, implying that overly aggressive optimization degrades performance. For λ_{bias}, the zero setting produces the broadest but generally most favorable distribution. λ_{bias}=0.5 tends to lower the median, while λ_{bias}=1.0 provides a partial recovery, especially over land. The dependence on CNN depth is more distinct: 5 layers gives the highest median performance over both land and ocean, while 4 layers is generally least favorable, indicating that the deeper architecture is beneficial for the present 7×7 patch configuration. By contrast, the dropout dependence is comparatively weak, with substantial overlap among all three values, although 0.5 tends to shift the distributions somewhat lower, especially over the ocean. Taken together, these results show that hyperparameter sensitivity is strongly coupled, so reliable model selection cannot be based on isolated trial runs. Instead, an ensemble of experiments is needed to identify robust high-performing configurations and to distinguish general tendencies from noise associated with individual training realizations.

https://doi.org/10.5194/egusphere-2026-4156
Preprint. Discussion started: 2 September 2026

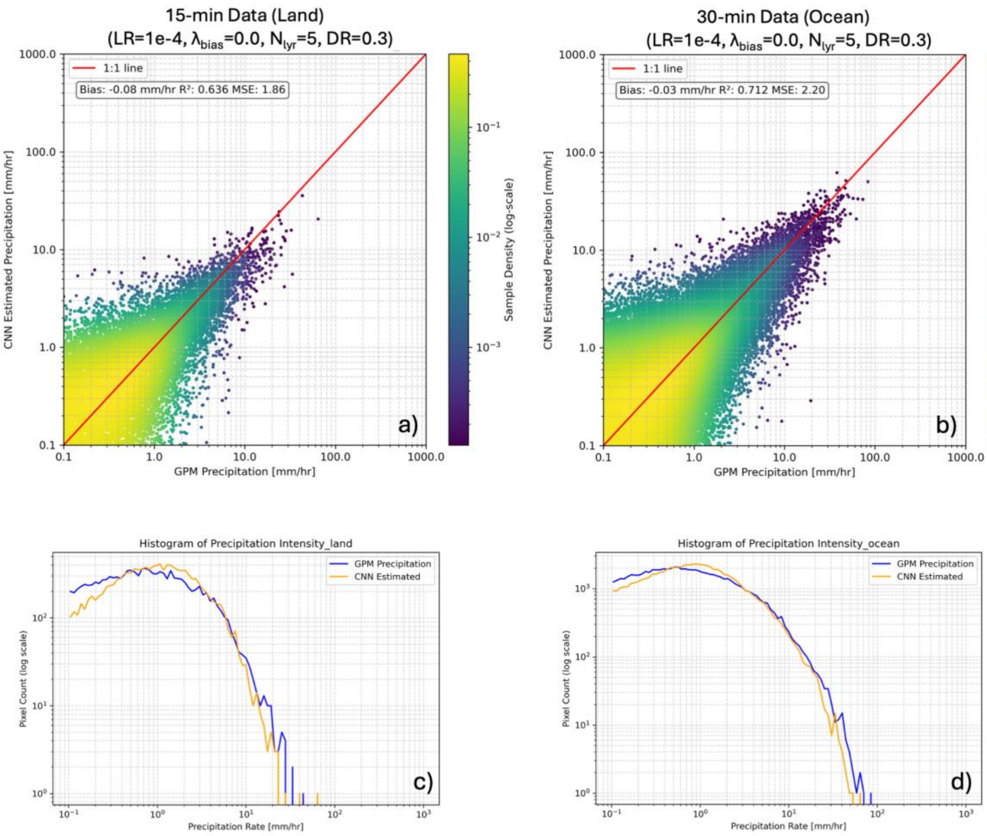

Figure 3: Scatter plots for the best CNN training models against GPM 2BCMB precipitation over a) land and b) ocean. The title shows 15-min (left) or 30-min (right) match-window datasets with the best sets of hyperparameters. Corresponding histograms of precipitation intensity over c) land and d) ocean.

The selected CNN training results are depicted with their precipitation-intensity histograms relative to GPM 2BCMB (Fig. 3). The land model in Fig. 3a is trained using the 15-min matchup database, while the ocean model in Fig. 3b is trained using the 30-min matchup database; these choices are made after evaluating their behavior in the full orbital retrieval products, as discussed later. In both panels, the densest part of the scatter lies close to the 1:1 line over the light-to-moderate precipitation range, indicating that the CNN captures the overall GPM precipitation structure reasonably well. The ocean model performs somewhat better than the land model in terms of correlation (R^2=0.712 versus 0.636), while both maintain only weak negative mean bias (−0.03

https://doi.org/10.5194/egusphere-2026-4156
Preprint. Discussion started: 2 September 2026

and −0.08 mm h^{-1}, respectively). As in many passive-microwave retrievals, both models show some compression of dynamic range, with light precipitation tending to be overestimated and heavier precipitation increasingly underestimated, as indicated by the tendency for high GPM rain rates to fall below the 1:1 line, particularly over land due to high emissivities and dynamic surface temperatures (Kidd et al., 2021a, 2021b).

The corresponding histograms in Figs. 3c and 3d further clarify the behavior of the selected models. Over land, the best CNN training reproduces the GPM 2BCMB precipitation distribution reasonably well over the light-to-moderate range, although the frequency of very light precipitation below 0.5 mm hr^{-1} is clearly underestimated. Over the ocean, the best CNN training provides a more consistent match to the GPM 2BCMB distribution, particularly across the dominant oceanic rain-rate regime, which is consistent with its reduced large-scale bias in the full orbital retrieval products.

CNN models trained with different temporal matchup databases (15 min versus 30 min) are not uniformly optimal when applied to final orbital retrievals because the spatial distribution of precipitation intensity differs substantially between land and ocean. This comparison also shows that intensity-dependent spatial bias, diagnosed from full orbital validation, is necessary for final model selection (not shown here). In particular, the 15-min matchup database yields the less-biased solution over land, whereas the 30-min matchup database yields the less-biased solution over ocean, probably because precipitation systems tend to have a shorter lifetime over land than over ocean (Futyan and Del Genio, 2007). An important advantage of the present ensemble CNN framework is that the land and ocean CNN retrievals are fully modularized, so the final system can readily adopt different optimal models over different surface types, and these components can be replaced, combined, or updated as improved statistical validation results become available.

https://doi.org/10.5194/egusphere-2026-4156
Preprint. Discussion started: 2 September 2026

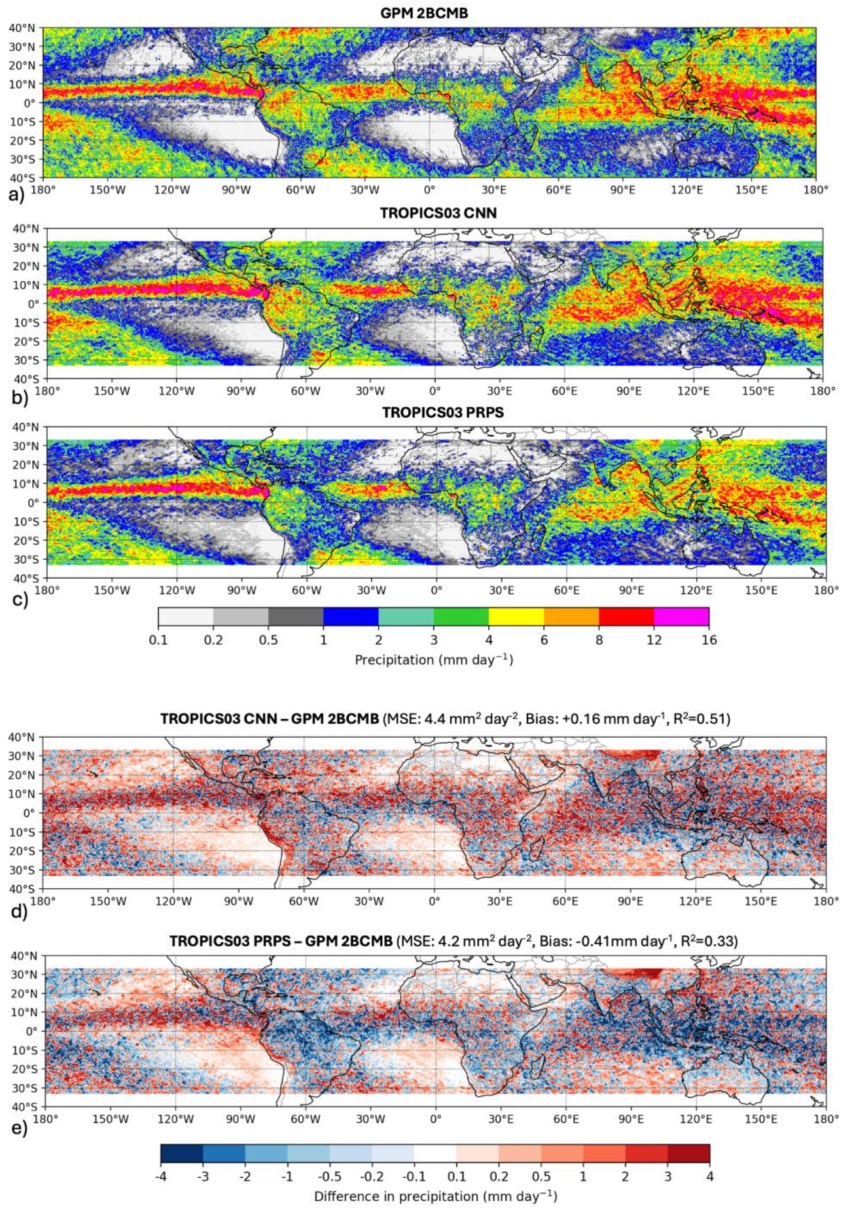

Figure 4: Climatological precipitation maps of a) GPM 2BCMB, b) TROPICS03 CNN, and c) TROPICS03 PRPS. Precipitation difference map between d) TROPICS03 CNN and GPM 2BCMB, and e) between TROPICS03 PRPS and GPM COMB. Each climatology is an integration

https://doi.org/10.5194/egusphere-2026-4156
Preprint. Discussion started: 2 September 2026

over 26 months from June 2023 to July 2025. TROPICS is sampled only within a 250 km swath width.

To compare TROPICS precipitation estimates (both CNN and PRPS) with GPM 2BCMB estimates, spots 36–46 from the central part of the swath are sampled in TROPICS products, corresponding to a swath width of roughly 250 km, so that the TROPICS sampling geometry is approximately matched to that of GPM. Figure 4 demonstrates that the TROPICS03 CNN retrieval reproduces the major climatological features of precipitation in comparison with GPM 2BCMB and TROPICS03 PRPS, including the zonally elongated ITCZ over the Pacific and Atlantic, enhanced rainfall over the Amazon, central Africa, the Maritime Continent, and monsoon regions of South and Southeast Asia. The overall spatially coherent structure indicates that the CNN can estimate a physically realistic distribution of tropical and subtropical precipitation from the TROPICS microwave observations.

The CNN-minus-GPM difference map in Fig. 4d shows that the residual biases are generally smaller-scale and more spatially heterogeneous than the large systematic departures seen in the PRPS-minus-GPM field in Fig. 4e. In particular, the CNN retrieval captures the broad tropical rainbands and continental convective maxima with relatively modest regional departures, although some organized biases remain over monsoon regions and parts of the tropical oceans. By contrast, the PRPS retrieval tends to underestimate precipitation more systematically over land, especially across tropical South America, Africa, and portions of the Maritime Continent. Over the ocean, PRPS also shows more widespread negative biases, particularly across the southern parts of the subtropical and midlatitude oceans. These patterns indicate that, at larger scales, the CNN retrieval provides a closer match to the observed spatial distribution of precipitation than the baseline PRPS retrieval. The bias (+0.16 mm day^{-1}) and R^2 (0.51) of CNN is better than those (bias: -0.41, R^2: 0.33) of PRPS. However, it should be noted that this version of the PRPS database is based on GPM passive-microwave precipitation, which is itself ultimately constrained by GPM 2BCMB precipitation. Even so, differences in the underlying database construction and matching procedure can still contribute to the regional biases evident here. One notable common feature is that both retrievals overestimate precipitation over the Tibetan Plateau and nearby high terrain. This suggests that complex topography and cold, high-elevation land surfaces remain challenging for

https://doi.org/10.5194/egusphere-2026-4156
Preprint. Discussion started: 2 September 2026

both methods. Nevertheless, this bias does not currently affect the LH CNN algorithm, because GPM CSH V7 retrievals are not performed over terrain elevations higher than 1000 m.

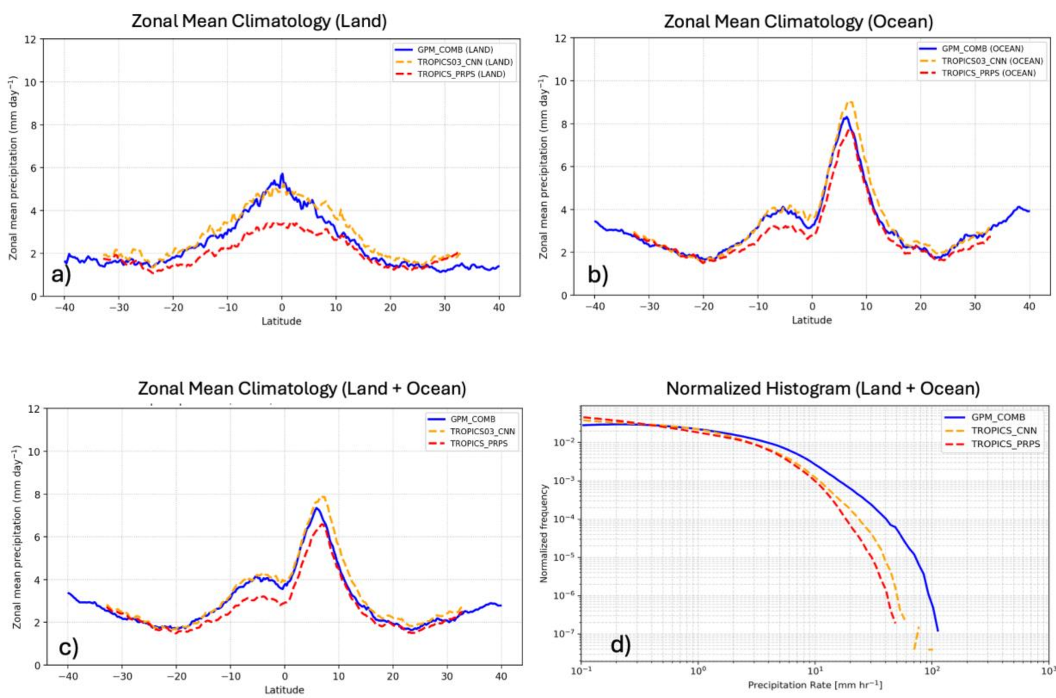

Figure 5. Zonally averaged precipitation climatology from GPM 2BCMB, TROPICS CNN, and PRPS over a) land, b) ocean, and c) land and ocean. (d) Normalized histograms of instantaneous precipitation intensities from full orbital data. Note that GPM 2BCMB precipitation (5km footprint size) is aggregated on a 25-km footprint size for this comparison.

Zonal composites and comparison further strengthen the interpretation from the spatial comparison (Fig. 5). Over land (Fig. 5a), TROPICS03 CNN captures both the tropical maximum and the subtropical minima reasonably well, whereas PRPS exhibits a systematic low bias across most tropical latitudes, especially near the equatorial peak. Over the ocean (Fig. 5b), both retrievals follow the broad zonal structure, but the CNN is generally closer to GPM 2BCMB overall, despite a slight overestimation between about 5° and 25°N. In contrast, PRPS remains systematically low from roughly 18°S to 7°N and again poleward of about 25°N. As a result, the combined land-plus-ocean climatology in Fig. 5c shows that the CNN reproduces the overall zonal structure of GPM

https://doi.org/10.5194/egusphere-2026-4156
Preprint. Discussion started: 2 September 2026

2BCMB more faithfully, although it still slightly overestimates the sharp tropical oceanic peak, whereas PRPS underestimates precipitation over most latitudes.

The normalized histogram in Fig. 5d shows that the CNN provides a modest improvement over PRPS in reproducing the frequency of heavy precipitation. However, this improvement remains limited, and both TROPICS retrievals still underrepresent the heaviest rain rates relative to GPM 2BCMB. This behavior likely reflects two factors. First, the information content of the available TROPICS sounder channels is inherently limited for the most intense precipitation regimes (section 3.3) by the lack of low frequency channels. Second, the CNN training database contains substantially fewer heavy-precipitation samples than are present in the full-orbital retrieval dataset, because the matchup-based training sample is much more restricted. Indeed, the reproduced frequency curve remains close to that seen in the training-based validation results (Fig. 3c and 3d). In the present study, the matchup database is limited to a 26-month period partly because of GPU memory constraints associated with the available NVIDIA V100 hardware. In future work, this limitation could be reduced by using larger-memory or newer-generation hardware (such as NVIDIA Grace Hopper), thereby allowing expansion of the training database and improved representation of rare heavy-precipitation events.

3.2 Latent Heating Training Results and Estimates

Similar to precipitation CNN ensemble selection, the composite Z-score is applied to choose the best LH CNN models. First, the vertical-skill statistics are averaged over the processed LH layer range of 1.0–12.5 km separately for land and ocean. For each ensemble member, mean vertical skill quantities such as mean R^2, mean MSE, and mean absolute bias are computed similarly to the precipitation CNN. In addition, due to unique vertical profile constraints, the mean negative-frequency bias (*NegFreqBias*) and mean negative-LH-amplitude bias (NegLHBias) are computed. *NegFreqBias* measures whether the CNN produces negative LH as often as the truth, while *NegLHBias* measures whether the amplitude of the predicted negative LH is too weak or too strong. The final composite score is then defined as,

https://doi.org/10.5194/egusphere-2026-4156
Preprint. Discussion started: 2 September 2026

$$Z_{tot}=Z(R^2) - Z(RMSE) - Z(|Bias|) - Z(|NegFreqBias|) - Z(|NegLHBias|). \quad \text{(Eq. 5)}$$

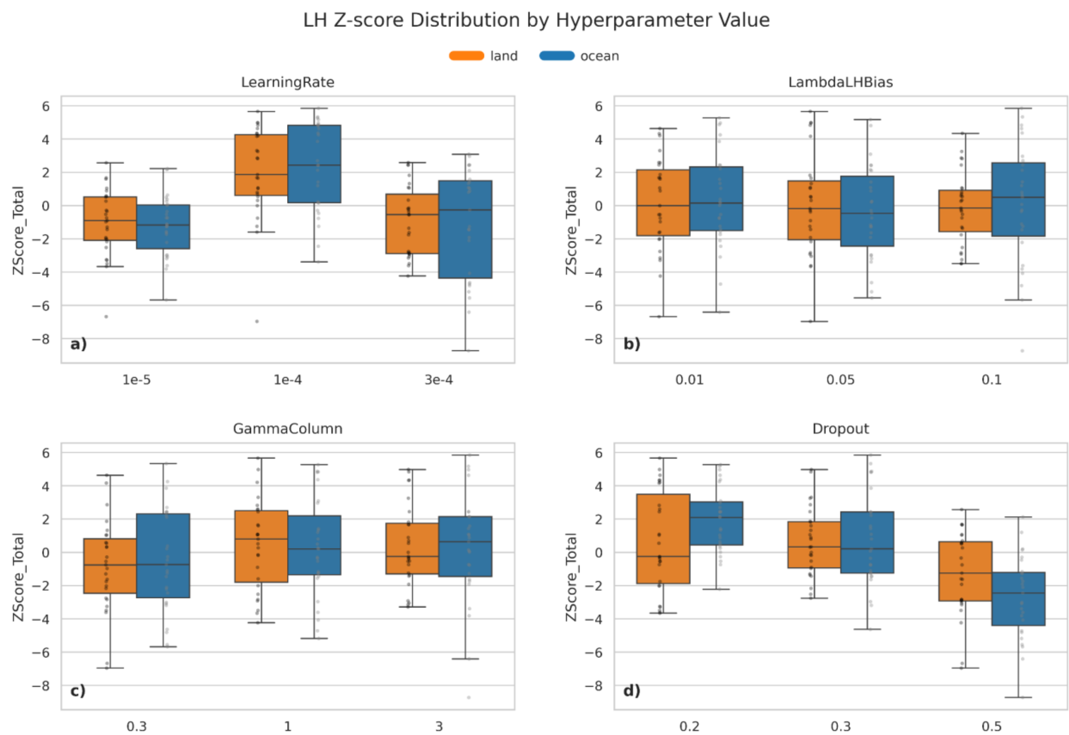

Figure 6: Box plots of Z_{tot} from each of the ensemble LH CNN-training members with respect to a) learning rate, b) column LH bias, c) precipitation-LH budget, and d) dropout ratio over land and ocean. The results are from GPM-TROPICS 15-min matchup data. Gray dots show the actual spread of Z_{tot}.

The sensitivity of the LH CNN skill, expressed by the combined Z-score, to the major hyperparameter groups over land and ocean is summarized in Fig. 6. Again, the ensemble still shows substantial spread within each hyperparameter category, indicating that the final LH skill depends on coupled interactions among these parameters. Both surface types exhibit broad distributions and several low-performing outliers, with the ocean in some cases showing comparably large or larger spread.

The learning-rate panel (Fig. 6a) shows the clearest and most systematic sensitivity. The smallest learning rate, 10^{-5}, generally produces negative or near-neutral median Z-scores for both land and ocean, indicating that this optimizer setting is too conservative for the LH profile problem. In contrast, 10^{-4} clearly shifts both land and ocean distributions upward and gives the highest median skill among the tested learning rates. The largest learning rate, 3×10^{-4}, performs less consistently. The LH-bias loss weight (Fig. 6b) shows weaker sensitivity than the learning rate. The three tested values, 0.01, 0.05, and 0.10, have strongly overlapping distributions for both land and ocean. There is a slight tendency for the ocean median to improve at 0.10, while the land median remains near neutral across the tested range. Similarly, the column-coupling strength (Fig. 6c) does not show a sharply separated optimum either. This indicates that the loose precipitation–LH coupling remains useful, but overly precise tuning of this weight is less important than choosing an appropriate learning rate.

The dropout panel (Fig. 6d) shows a more distinct sensitivity. Dropout values of 0.2 and 0.3 generally produce the best central tendencies, while 0.5 shifts both land and ocean distributions downward. The degradation is especially clear over the ocean, where the median Z-score becomes strongly negative, and several low-performing cases appear. This suggests that excessive regularization removes information needed to reconstruct the vertical LH structure, including weak negative heating/cooling features.

https://doi.org/10.5194/egusphere-2026-4156
Preprint. Discussion started: 2 September 2026

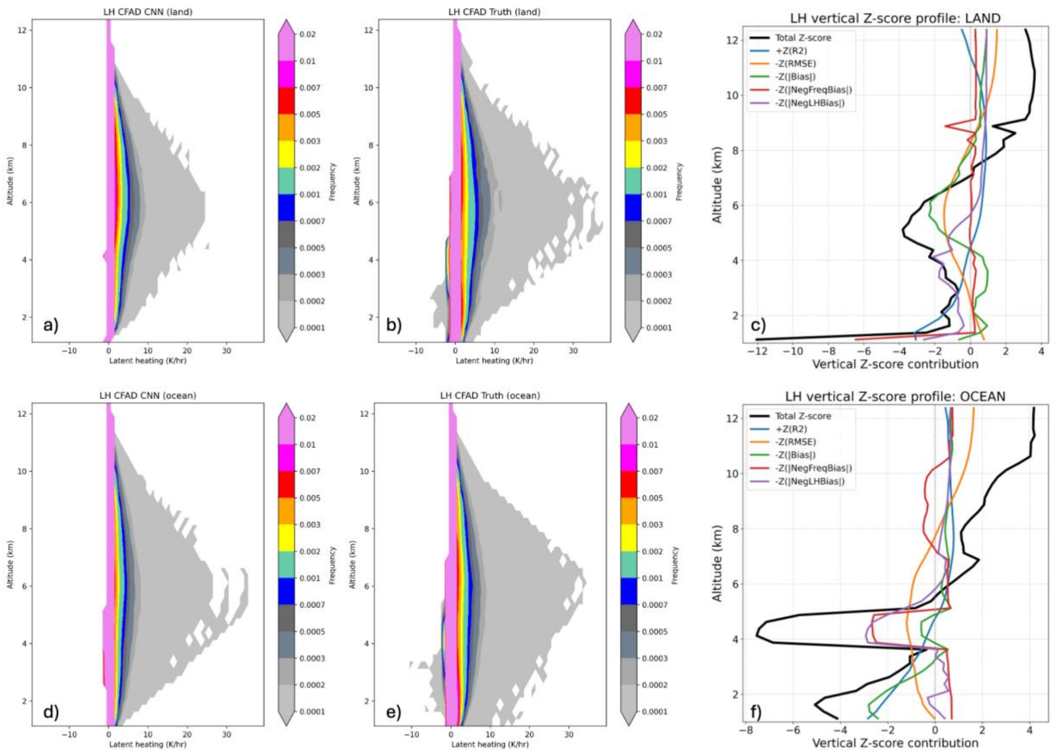

Figure 7. LH CFADs from the best LH CNN models over a) land and d) ocean, as well as corresponding GPM CSH LH CFADs (truth) over b) land and e) ocean. Vertical profiles of Z-score and component contributions over c) land and f) ocean.

The LH vertical distributions from the best CNN retrievals are compared with the corresponding GPM CSH retrievals over land and ocean in Fig. 7. Overall, the CNN reproduces the primary positive-heating structure reasonably well in both regimes. Over land, the CNN CFAD captures the main positive LH mode extending from the lower troposphere to about 10–11 km, with the largest occurrence centered in the mid-troposphere. Over the ocean, the CNN also reproduces the broad positive-heating envelope. This indicates that the LH CNN successfully learns the dominant heating structure associated with precipitating convection.

However, important differences remain in the weak negative-LH portion of the distributions. The "truth" CFADs show persistent weak negative LH, especially below roughly 6–7 km. This feature is physically expected because melting and evaporation under stratiform regions can produce

https://doi.org/10.5194/egusphere-2026-4156
Preprint. Discussion started: 2 September 2026

577 broad, weak negative heating below and around the melting layer. The CNN captures some of this negative LH, but its distribution is more compressed and less broadly spread than the truth, even if the LH CNN model adds penalty terms to represent them better.

The vertical Z-score profiles (Figure 7c and 7d) facilitate identifying which skill components control these errors. Over land, the total Z-score shows a large negative excursion near the lowest processed level. This degradation is contributed to by several terms, especially the negative-frequency and negative-LH-bias components, indicating that the CNN model struggles to reproduce the occurrence and amplitude of weak cooling near the lower boundary of the retrieval layer. Above about 7 km, the land Z-score becomes positive, implying that upper-level heating skill is relatively strong, consistent with the fact that the TROPICS channels are sensitive to the scattering by ice particles aloft but not liquid precipitation at lower levels. Over the ocean, the most prominent negative Z-score occurs around 4–5 km. The negative-frequency and negative-LH-amplitude terms strongly contribute to this minimum, confirming that the main ocean weakness is not simply total RMSE or mean bias, but specifically the underrepresentation or vertical misplacement of persistent weak negative LH near the melting layer.

https://doi.org/10.5194/egusphere-2026-4156
Preprint. Discussion started: 2 September 2026

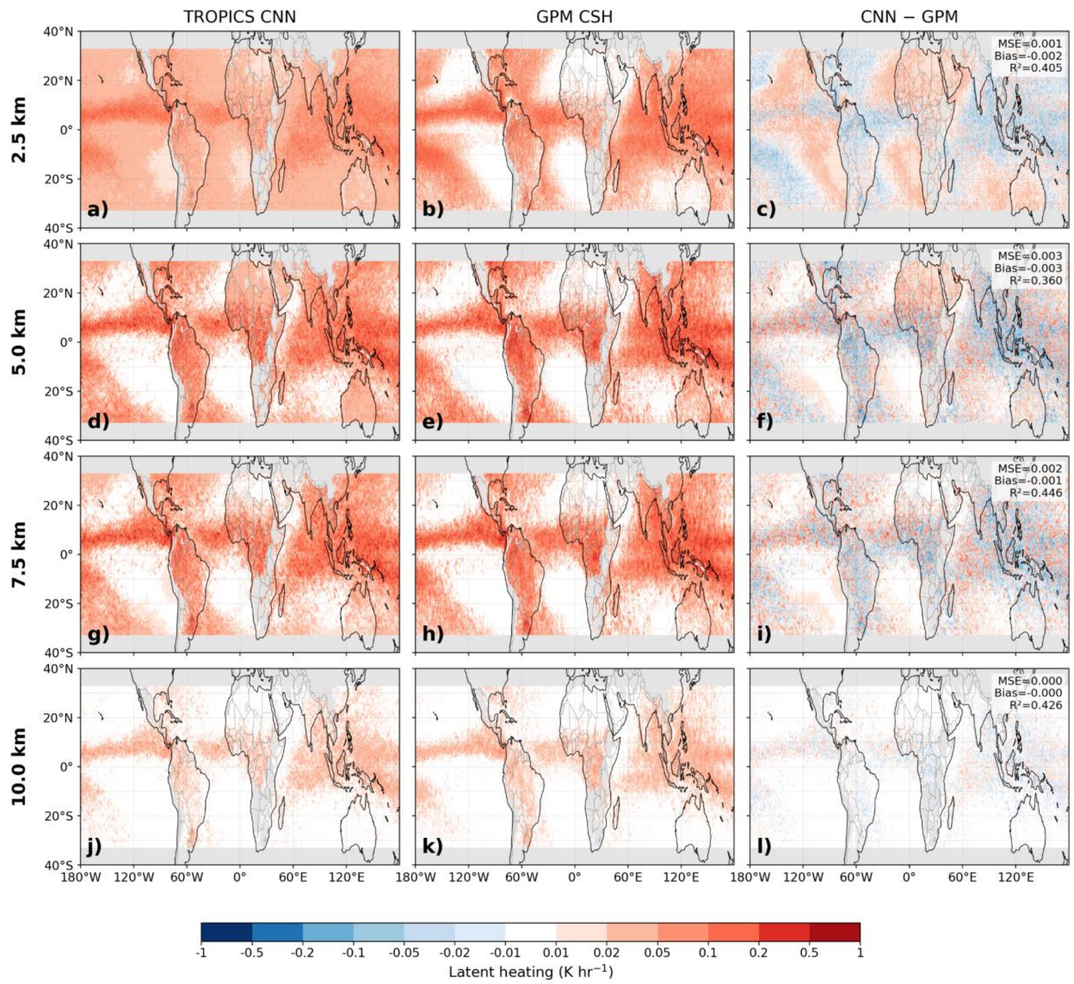

Figure 8. Mean LH maps at 2.5, 5.0, 7.5, and 10.0 km over 26 months from June 2023 to July 2025. The left column shows TROPICS CNN retrievals, the center column shows GPM CSH, and the right column shows their differences (TROPICS CNN minus GPM CSH). Regions with terrain elevations greater than 1 km are excluded from both the retrieval and the analysis.

The TROPICS CNN reproduces the broad climatological structure of LH observed in GPM CSH at all four selected levels (Fig. 8), while also revealing several altitude-dependent biases. At 2.5 km (Fig. 8a–c), both products show widespread weak positive heating across much of the tropics and subtropics, but the difference field indicates that the CNN tends to underestimate LH in regions of stronger CSH heating and overestimate LH in areas of weak to negligible heating in CSH,

https://doi.org/10.5194/egusphere-2026-4156
Preprint. Discussion started: 2 September 2026

particularly in low-cloud regions over the ocean off the west coasts of continents. This LH overestimation is also associated with the inability of the precipitation CNN to accurately reproduce light precipitation rates in this region, with the CNN generally overestimating light precipitation (Fig. 4). The bias is also indicated with the large Z-score profile at 2.5 km height over ocean (Fig. 7f).

At 5.0 and 7.5 km (Fig. 8d–i), the agreement is strongest: both datasets capture the pronounced zonal tropical heating belt, enhanced continental heating over the Amazon, Africa, and the Maritime Continent, and broad maxima over the Indo-Pacific region. These middle levels also contain the largest climatological heating magnitude, suggesting that they correspond to the core layer of LH release from deep convective systems. The CNN–GPM difference panels show that the remaining biases at these levels are generally regional and moderate in amplitude rather than gross structural failures, which indicates that the CNN has learned the dominant spatial organization of tropical heating associated with surface precipitation rates (Figure 4). At 10.0 km (Fig. 8j–l), the LH signal becomes weaker in both products, and the CNN continues to follow the overall tropical distribution. This mid-to-upper-level heating is a more critical driver for tropical large-scale circulation (e.g., Hartmann et al., 1984).

https://doi.org/10.5194/egusphere-2026-4156
Preprint. Discussion started: 2 September 2026

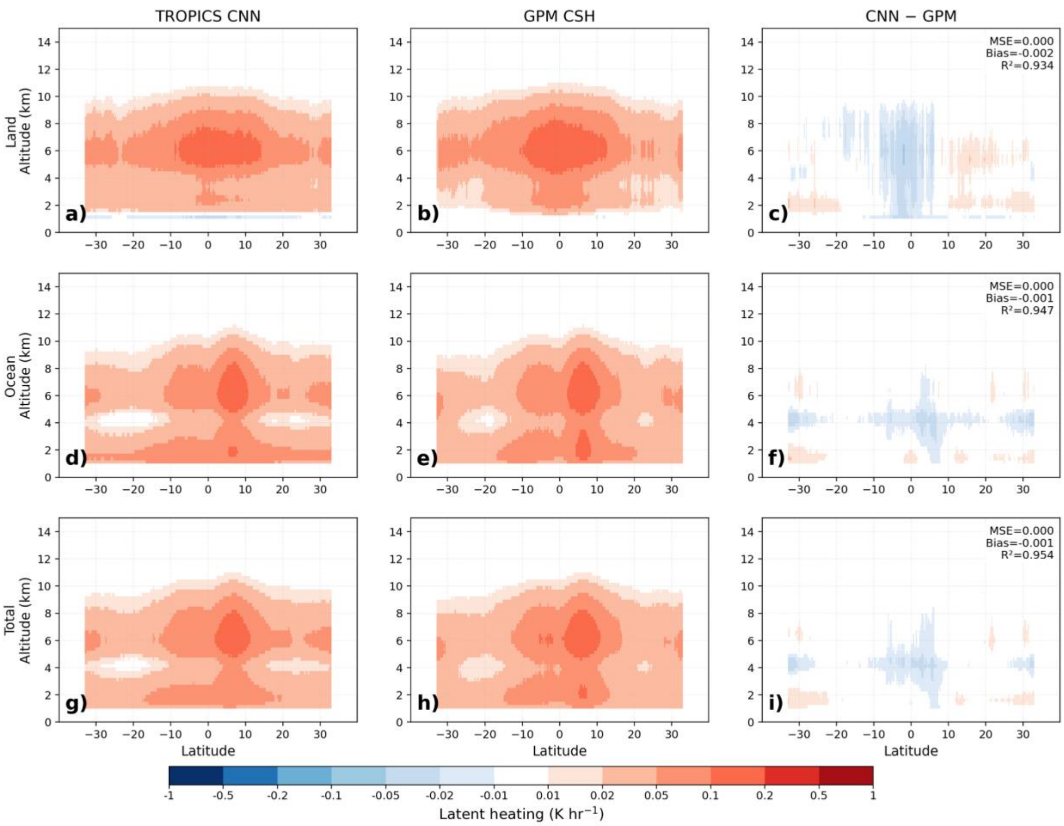

Figure 9. Climatology of zonally averaged LH profiles corresponding to Fig. 8. The top row shows results for over land, the middle row for over ocean, and the bottom row for both land and ocean. The left and middle columns show the mean LH profiles for the TROPICS CNN and GPM CSH, respectively, while the right row shows the difference (TROPICS – GPM) and related statistics.

Zonally averaged LH climatologies are shown corresponding to the spatial maps of Fig. 8 (Fig. 9). Over land (Fig. 9a–c), both products show a deep layer of positive heating extending from roughly 2 to 10 km, with the strongest heating centered near 5–7 km and broadly distributed across the Tropics. Over the ocean (Fig. 9d–f), the same general vertical structure is evident, but with more clearly defined ITCZ maxima in the deep tropics and minima in the subtropics, and a more prominent low-level secondary maximum. The combined land-plus-ocean climatology (Fig. 9g–i)

https://doi.org/10.5194/egusphere-2026-4156
Preprint. Discussion started: 2 September 2026

preserves these same large-scale features, indicating that the CNN captures the dominant zonal–vertical distribution of LH across the tropical belt.

The difference panels reveal that the largest discrepancies are concentrated mainly in the middle troposphere, particularly around 4–8 km, and near equatorial to low-latitude tropical regions. Over land, the CNN tends to be weaker than GPM CSH in the core midlevel heating layer, especially near the equator, while small positive differences appear at some subtropical latitudes and at lower levels. This lower-level bias is indicated by the Z-score vertical profile over land (Fig. 7c, green line). Over ocean, the CNN-minus-GPM structure shows a similar tendency toward reduced heating in the tropical mid-troposphere, although the differences are somewhat more confined around the 4-km level, just below the typical tropical melting level. This pattern is in agreement with the prominent negative Z-score around 4-5 km over ocean during the CNN training (Fig. 7f). In the combined field, the over-ocean LH profile dominates the overall bias signals, implying that the CNN slightly underestimates the strongest portion of the climatological heating core even while reproducing its overall location and shape.

3.3 Channel and Patch Importance to Precipitation and LH Retrievals

This section examines the relative contribution of each TROPICS channel and Tb patch to the trained CNN retrievals. By quantifying channel- and patch-dependent sensitivities, this analysis helps interpret how the otherwise complex CNN algorithm uses TROPICS microwave Tb information to constrain the variability of precipitation and the vertical structure of LH.

https://doi.org/10.5194/egusphere-2026-4156
Preprint. Discussion started: 2 September 2026

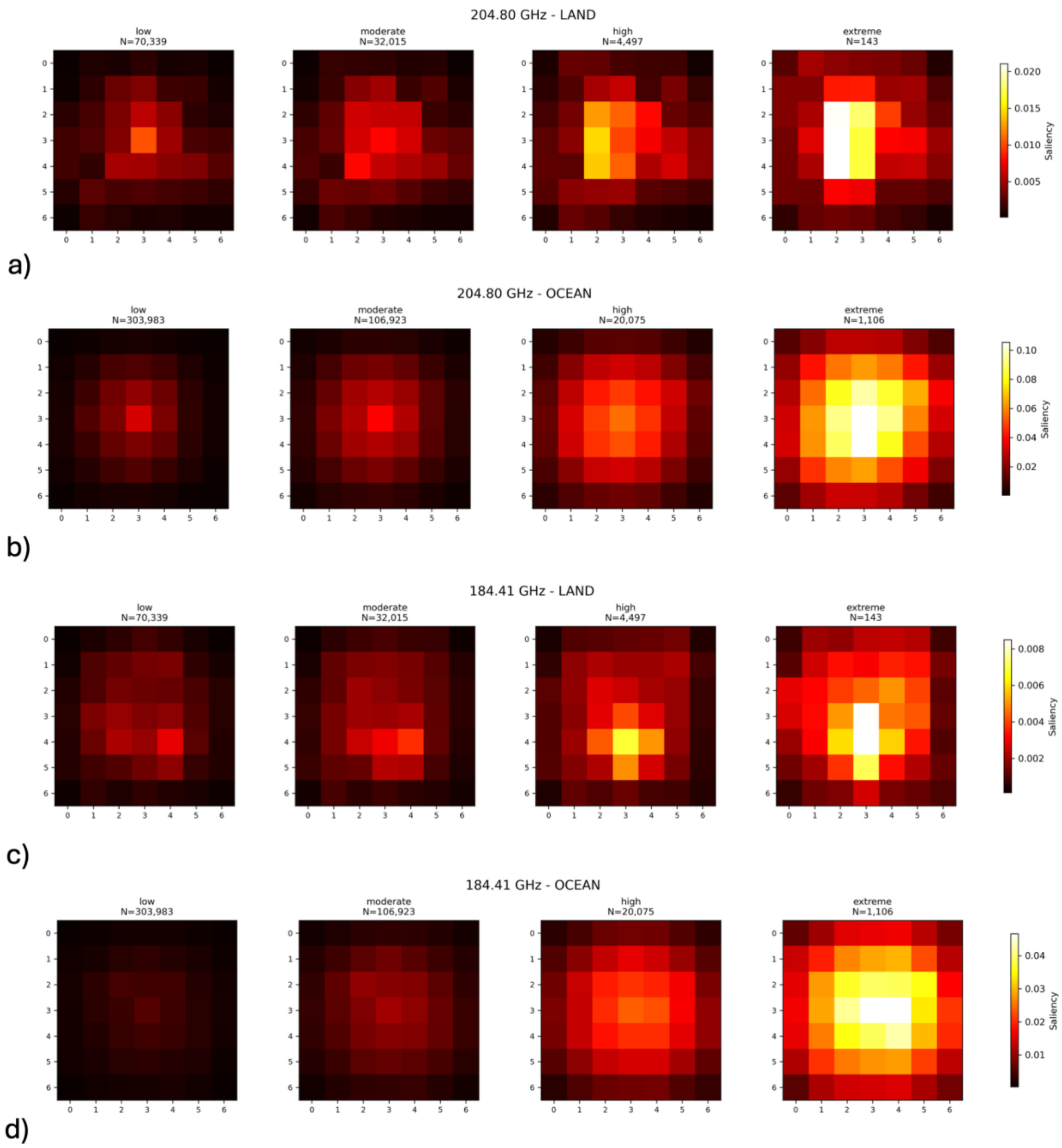

Figure 10: (a, b) CNN mean local gradient of 7×7 Tb patches (*saliency*) from the 204.8 GHz channel over a) land and b) ocean, grouped by low (0.1 ~ 1.0 mm hr^{-1}), moderate (1.0 ~ 5.0 mm hr^{-1}), high (5.0 ~ 20.0 mm hr^{-1}), and extreme (20.0 ~ 100 mm hr^{-1}) rain rate categories. (c, d) Similar diagrams but from the 184.41 GHz channel over c) land and d) ocean. N represents sample numbers.

https://doi.org/10.5194/egusphere-2026-4156
Preprint. Discussion started: 2 September 2026

For the precipitation retrieval, local-gradient analysis is used to quantify the sensitivity of the trained CNN output to individual TROPICS Tb inputs within the 7×7 Tb patch (*saliency* hereafter for convenience). After estimation of the CNN precipitation rate for a given input patch, the gradient of the predicted rain rate with respect to each input channel and patch location is calculated by backpropagation. The magnitude of this gradient indicates how strongly a small perturbation in a given Tb value would affect the retrieved precipitation. Larger gradient magnitudes therefore identify channels and spatial locations that exert stronger local control on the CNN precipitation estimate, whereas smaller values indicate weaker sensitivity. By averaging these gradients over many samples and stratifying them by precipitation intensity, the analysis reveals how the CNN uses different microwave channels and surrounding spatial texture under different rain regimes.

CNN saliency values are then composited within precipitation-intensity categories (Fig. 10): low to extreme precipitation categories. Thus, larger saliency indicates patch locations where small perturbations in Tb would have a stronger local influence on the CNN precipitation estimate. Based on the previous figure, patterns associated with one of the most (least) sensitive channels, 204.8 GHz (184.4 GHz), are highlighted.

The 204.8 GHz channel shows a pronounced maximum near the center of the patch, especially for low and moderate precipitation, indicating that the CNN relies most strongly on Tb information near the collocated precipitation target. As precipitation intensity increases, the sensitivity becomes broader and extends into neighboring pixels. This broadening is physically reasonable because heavier precipitation is more often associated with spatially organized convective systems, including mesoscale convective systems, where surrounding ice-scattering signatures provide useful information for heavy precipitation. The 184.4 GHz channel shows generally weaker and more diffuse saliency than 204.8 GHz, suggesting that it contributes less directly to the local precipitation estimate, particularly for weaker precipitation regimes.

These saliency maps also support the use of a 7×7 CNN patch for this retrieval problem. In most panels, the patch edges exhibit much smaller saliency than the central and near-central pixels, implying that most of the useful spatial information is contained well within the 7×7 window. The main exception appears in the extreme precipitation category, where saliency becomes broader and can extend closer to the patch edges. However, this category has extremely smaller sample numbers (~ 0.014%) than the low, moderate, and high categories, so its spatial pattern is less statistically robust. Overall, the results confirm that the 7×7 patch is generally sufficient for capturing the dominant local Tb structures used by the CNN, while larger patches may only provide additional value for rare, highly organized extreme-precipitation scenes. However, a larger input patch would further increase GPU memory use and computational cost. For example, expanding the patch size from 7×7 to 8×8 increases the number of input pixels by about 31%, which will reduce the number of training samples for a given GPU memory size.

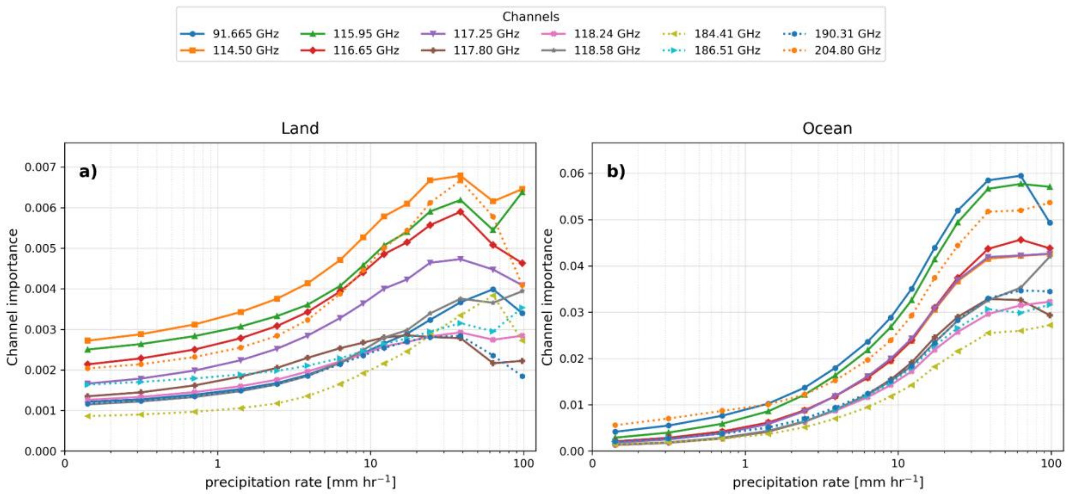

Figure 11. Channel importance of precipitation CNN to the precipitation intensity spectrum over (a) land and (b) ocean.

A channel-importance analysis using the trained TROPICS CNN precipitation retrieval models is performed. Namely, the local derivative of the CNN output is calculated with respect to each input 7×7 Tb element. The absolute value of this derivative is then averaged over the 7×7 patch to obtain a single channel-importance value and is composited for each precipitation intensity bin. Again, in this sense, the plotted quantity (channel importance) does not represent the magnitude of the Tb itself, but rather the local sensitivity of the trained CNN retrieval to small perturbations in Tb for each channel. Note that this index represents the sensitivity of each channel as an independent source of information and does not account for correlations among different channels.

https://doi.org/10.5194/egusphere-2026-4156
Preprint. Discussion started: 2 September 2026

The results indicate that the CNN uses different spectral information over land and ocean (Fig. 11). Over land, channel importance is relatively low for light precipitation and increases rapidly for moderate-to-heavy precipitation, confirming that the land model relies more strongly on scattering signatures associated with deeper and more intense precipitating systems. The largest land sensitivities occur mainly in the oxygen-band channels near 114–117 GHz and the 204.80 GHz channel. In contrast, channels around 183 GHz are among the least sensitive over most precipitation intensities, but these sensitivities vary slightly between moderate-to-heavy precipitation. Over ocean, the channel sensitivities are one order larger than those of land, suggesting more robust precipitation retrieval over ocean. The most sensitive channels for heavy precipitation are 91.665, 116.65, and 204.8 GHz, whereas the 184.41 GHz channels remain among the least sensitive again. For light precipitation, ocean sensitivities are already appreciable in 91.665, 114.50, and 116.65 GHz, consistent with the greater microwave emissivity contrast over ocean surfaces and the stronger relationship between low-frequency Tb perturbations and precipitation-related signals.

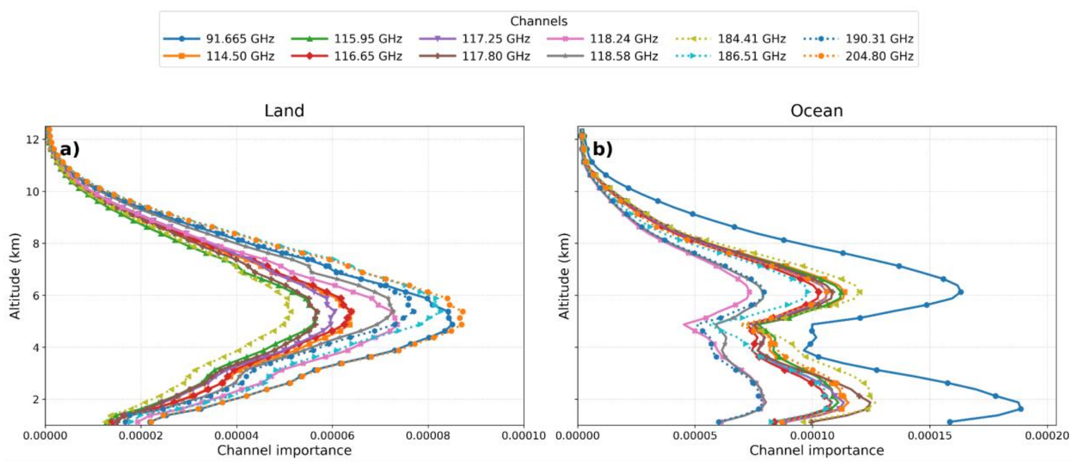

Figure 12: Vertical profile of channel importance to LH CNN over a) land and b) ocean.

https://doi.org/10.5194/egusphere-2026-4156
Preprint. Discussion started: 2 September 2026

Similar to the precipitation analysis, vertical profiles of channel importance are calculated from the trained LH CNN. Figure 12 shows vertical profiles of channel importance over land and ocean. Over land, the channel-importance profiles show a broad maximum in sensitivity peaking near 5–6 km. This altitude range corresponds to the mixed-phase region, where passive microwave channels are strongly influenced by scattering from ice-phase hydrometeors. Most channels have very similar vertical shapes: weak sensitivity near 1–2 km, increasing upward toward the mid-troposphere, and then decreasing rapidly above about 9–10 km. This broadly represents the general magnitude of actual LH profiles over land and ocean (Fig. 7).

An interesting feature is that the 184–190 GHz channels exhibit some of the strongest sensitivity in the LH CNN, although these channels have the weakest importance in the precipitation CNN (Figs. 11a and 12a). These channels are sensitive to water vapor absorption and ice scattering, so their strong contribution around 5–7 km is physically reasonable. The 91.655 GHz channel contributes a similar magnitude, but does not dominate over land, compared with the ocean (Fig. 12b). This may reflect the more complicated and variable land surface emissivity background and column water vapor, which reduces the usefulness of lower-frequency surface-sensitive channels for LH CNN over land.

Over the ocean (Fig. 12b), the structure is quite different. The 91.655 GHz channel appears to be the most critical channel among others, especially around 6 km and again near the lower-tropospheric peak around 1.5–2.5 km. This is physically plausible because ocean surfaces have relatively low and more uniform microwave emissivity, providing stronger information about precipitation-sized hydrometeors and column rain structure. It is also interesting that the 184.41 GHz channel is the second most important channel, which is opposite to the over-land case (Fig. 12a). On the other hand, 118.24, 118.58, and 190.31 channels are the weakest channels over the ocean. The ocean profiles also show a minimum around 4-5km, which corresponds to a low Z-score value at this altitude in the CNN training (Figure 7f), suggesting LH values around this altitude are less sensitive to variability of microwave Tbs. The 91.665 GHz sensitivity below 3 km may be related to warm-rain and low-level precipitation structure, which is better observed over the ocean than over land because of the cleaner microwave surface background.

https://doi.org/10.5194/egusphere-2026-4156
Preprint. Discussion started: 2 September 2026

While both domains show maximum sensitivity in the mid-troposphere, the main difference is that land uses a more distributed set of channels with comparable contributions, whereas the ocean is more strongly controlled by 91.665 GHz channel. This contrast is somewhat consistent with the channel importance for precipitation, where 91.665 GHz channel is less important over the land, but more critical over the ocean (Fig. 11) most likely due to the different microwave radiative backgrounds over land and ocean; i.e., land retrievals must rely more on scattering and water-vapor channels, while ocean retrievals can exploit lower-frequency scattering signatures more effectively. In addition, the larger footprint sizes of lower-frequency TROPICS channels could degrade Tb sensitivity to precipitation and LH over land, where continental precipitation systems generally occur at smaller spatial scales (Nesbitt et al., 2000).

3. Summary and Future Direction

This study develops a two-step ensemble CNN framework to retrieve surface precipitation and LH profiles from TROPICS passive-microwave observations using GPM-based products as training targets. In the first step, a precipitation CNN is trained with collocated TROPICS brightness temperatures and GPM 2BCMB precipitation. The ensemble CNN experiments show that retrieval skill is largely controlled by the interaction among optimizer settings, architecture depth, and loss weighting rather than by any one hyperparameter in isolation. Although some configurations produce favorable pointwise validation statistics, the final orbital-scale evaluation demonstrates that internal training metrics alone are not sufficient for model selection due to unique distributions of precipitation intensity across tropical environments. In particular, the 15-min matchup database yields a less biased land retrieval, whereas the 30-min matchup database yields a less biased ocean retrieval, indicating that the optimal solution depends not only on nominal validation skill but also on the large-scale spatial and intensity distributions that emerge in the full retrieval product. Overall, the precipitation CNN reproduces the large-scale climatological structure of GPM 2BCMB much better than the baseline PRPS retrieval, including the main tropical rainbands and zonal-mean maxima, although the heaviest rain-rate frequencies remain underrepresented due to a limited CNN training sample volume at higher rates.

https://doi.org/10.5194/egusphere-2026-4156
Preprint. Discussion started: 2 September 2026

In the second step, the same TROPICS Tb patch information is used to retrieve LH vertical profiles from 1 to 12 km altitude, with the precipitation retrieval providing an additional physical constraint through the precipitation–LH budget linkage. The LH CNN ensemble analysis shows that learning rate and dropout exert the clearest influences on skill, while the LH-specific loss weights associated with column bias and precipitation–LH consistency are less sharply sensitive within the tested ranges. The resulting LH climatologies are compared favorably with GPM CSH in both horizontal maps and zonal-mean vertical structure. The TROPICS CNN reproduces the broad tropical heating maxima, their mid-tropospheric placement, and their meridional extent over land, ocean, and the combined domain. The best agreement occurs near the main heating layer near 5–7.5 km, but agreement tends to worsen around the melting layer over the ocean and near the surface over land. Zonal profiles indicate that the CNN LH tends to be somewhat weaker than that of GPM CSH, especially in equatorial regions. Despite the limited single-footprint information content of the TROPICS sounder, the two-step ensemble CNN framework can recover physically reasonable climatological LH structure in addition to surface precipitation.

The interpretation of these results is strengthened by the channel-importance and saliency analyses. Those diagnostics show that the CNN does not behave as a purely pixel-wise nonlinear regression, but instead uses the spatial structure of the 7×7 Tb patch in a way that is physically plausible. For precipitation retrieval, the local-gradient analysis shows the strongest sensitivity near the patch center, with broader spatial influence for heavier rain rates and smaller contributions toward the patch edges. This confirms that 7×7 Tb patches, approximately representing the mean size of tropical MCSs (~200 km; Chen and Houze, 1996, 1997), are suitable for maximizing benefits from the CNN training. For LH retrieval, the channel-gradient analysis indicated that the CNN relies on different combinations of scattering and sounding information over land and ocean. These analyses suggest that the trained network is extracting meaningful convective structure from the TROPICS observations rather than merely fitting statistical noise, which increases confidence in the physical interpretability of the retrievals.

The present results are broadly consistent with the recent shift in passive-microwave retrieval research from pixel-wise methods toward spatially aware neural-network frameworks (e.g.,

https://doi.org/10.5194/egusphere-2026-4156
Preprint. Discussion started: 2 September 2026

Sadeghi et al., 2019; Li et al., 2021; Pfreundschuh et al., 2022; Afzali Gorooh et al., 2023; Gavahi et al., 2023; Cannon et al., 2026). In addition, this research demonstrates that smallsat passive microwave sounder channels trained with CNN techniques can provide realistic LH vertical profiles in addition to standard atmospheric products, while improving the biases typically associated with light and heavy precipitation regimes over the existing product. This is a particularly important extension for TROPICS because the scientific motivation of the mission is tied not only to storm environment and rainfall monitoring, but also to the evolution of tropical convection and its role in the broader atmospheric energy cycle.

Several future directions follow naturally from this study. First, the present matchup database is limited in part by the memory and throughput constraints of the available NVIDIA V100 GPU hardware. This limitation likely contributes to the underrepresentation of infrequent heavy-precipitation events in the training sample. Migration to newer GPU systems such as Grace Hopper should allow substantially larger training datasets, faster ensemble exploration, and more complete sampling of extreme precipitation. Second, the framework can be expanded from the TROPICS data investigated here to Tomorrow.io sounders (Munchak et al., 2025) because of their very similar channel configuration and weighting-function behavior. This provides a natural path toward extending the present ML framework beyond TROPICS itself and toward broader operational application using a denser mixed constellation of microwave sounders in the near future. Finally, once frequent precipitation and LH retrievals are available from such constellations, they can be combined with radiative-heating estimates to examine radiative–convective energy closure more directly. Namely, this would provide a new observational basis for studying how precipitation, LH, radiative cooling, and tropical convective organization evolve together, thereby advancing understanding of tropical weather systems and their role in climate.

Code availability: The Python-based two-step CNN retrieval algorithm is developed using the PyTorch framework. CNN training, retrieval, and Z-score analysis and plotting codes are available from the NASA NCCS Dataportal at [https://portal.nccs.nasa.gov/datashare/cloudlibrary/PUB_DATA/TROPICS_CNN_2026/SOFT].

https://doi.org/10.5194/egusphere-2026-4156
Preprint. Discussion started: 2 September 2026

Data availability: TROPICS L1 brightness temperature products and GPM 2BCMB and CSH products are publicly available through NASA Earthdata at [https://www.earthdata.nasa.gov/]. CNN-derived precipitation-LH L2 product files are available from the NASA NCCS Dataportal at [https://portal.nccs.nasa.gov/datashare/cloudlibrary/PUB_DATA/TROPICS_CNN_2026/L2/].

Author contribution: TM designed the study, developed the CNN framework, performed the analysis, and prepared the manuscript. SB and SR contributed to the scientific interpretation and manuscript revision.

Competing interests: The authors declare that they have no conflict of interest.

Acknowledgement: This project is funded by the TROPICS mission led by principal investigator Dr. William Blackwell. The authors especially acknowledge the lifelong contributions of Dr. Wei-Kuo Tao to the development of satellite-based LH products, as well as his mentorship over the past several decades at NASA Goddard Space Flight Center. All computations are carried out on the NASA NCCS PRISM GPU clusters. Large Language Model (LLM) tools are used for grammatical corrections and code development.

https://doi.org/10.5194/egusphere-2026-4156
Preprint. Discussion started: 2 September 2026

References:

Afzali Gorooh, V., Petković, V., Arulraj, M., Nguyen, P., Hsu, K., Sorooshian, S., and Ferraro, R. R.: Integrating LEO and GEO observations: Toward optimal summertime satellite precipitation retrieval, J. Hydrometeorol., 24, 1939–1954, https://doi.org/10.1175/JHM-D-23-0006.1, 2023.

Blackwell, W. J., Braun, S. A., Leslie, R. V., Piepmeier, J. R., Chappell, W. J., and Barnet, C. D.: An overview of the TROPICS NASA Earth Venture mission, Q. J. Roy. Meteorol. Soc., 145, 3200–3214, https://doi.org/10.1002/qj.3588, 2018.

Blackwell, W. J., Braun, S. A., Alvey, G. R., Atlas, R., Bennartz, R., Braun, J., Cahoy, K., Chen, R., Chirokova, G., Dahl, B., Darlow, J., DeMaria, M., Diliberto, M., Dunion, J., Duran, P., Greenwald, T., Griffin, S., Griffith, Z., Herndon, D., Hawkins, J., Kalluri, S., Kidd, C., Kim, M. J., Leslie, R. V., and co-authors: High revisit-rate tropical cyclone observations from the NASA TROPICS satellite constellation mission, Proc. IEEE, https://doi.org/10.1109/JPROC.2025.3582502, 2025.

Cannon, F., and co-authors: Deep learning for multisatellite precipitation retrievals: Impact of Tomorrow.io's microwave sounders, J. Hydrometeorol., 27, 453–471, https://doi.org/10.1175/JHM-D-25-0007.1, 2026.

Chen, S. S. and Houze, R. A.: Diurnal variation and life-cycle of deep convective systems over the tropical Pacific warm pool, Q. J. Roy. Meteorol. Soc., 123, 357–388, 1997.

Chen, S. S. and Houze, R. A.: Mesoscale convective systems and stratiform rainfall in a satellite and rain gauge analysis of TOGA COARE, Mon. Weather Rev., 124, 2700–2713, 1996.

Chen, X., Stubenrauch, C. J., and Mandorli, G.: Relationship between latent and radiative heating fields of tropical cloud systems using synergistic satellite observations, Atmos. Chem. Phys., 25, 6857–6880, https://doi.org/10.5194/acp-25-6857-2025, 2025.

Chou, C. and Neelin, J. D.: Mechanisms of global warming impacts on regional tropical precipitation, J. Climate, 17, 2688–2701, https://doi.org/10.1175/1520-0442(2004)017<2688:MOGWIO>2.0.CO;2, 2004.

Futyan, J. M. and Del Genio, A. D.: Relationships between deep convective system properties and development from geostationary satellite data, J. Climate, 20, 1544–1601, https://doi.org/10.1175/JCLI4084.1, 2007.

Gavahi, K., Foroumandi, E., and Moradkhani, H.: A deep learning-based framework for multi-source precipitation fusion, Remote Sens. Environ., 295, 113723, https://doi.org/10.1016/j.rse.2023.113723, 2023.

Gill, A. E.: Some simple solutions for heat-induced tropical circulation, Q. J. Roy. Meteorol. Soc., 106, 447–462, https://doi.org/10.1002/qj.49710644905, 1980.

Glorot, X., Bordes, A., and Bengio, Y.: Deep sparse rectifier neural networks, in: Proceedings of the 14th International Conference on Artificial Intelligence and Statistics, Fort Lauderdale, FL, USA, 11–13 April 2011, 315–323, 2011.

Grecu, M., Olson, W. S., Munchak, S. J., Ringerud, S., Liao, L., Haddad, Z. S., Kelley, B. L., and McLaughlin, S. F.: The GPM combined algorithm, J. Atmos. Ocean. Tech., 33, 2225–2245, https://doi.org/10.1175/JTECH-D-16-0019.1, 2016.

Grecu, M., Olson, W. S., Shie, C.-L., L'Ecuyer, T. S., and Tao, W.-K.: Combining satellite microwave radiometer and radar observations to estimate atmospheric latent heating profiles, J. Climate, 22, 6356–6376, https://doi.org/10.1175/2009JCLI3020.1, 2009.

Hagos, S. and Zhang, C.: Diabatic heating, divergent circulation and moisture transport in the African monsoon system, Q. J. Roy. Meteorol. Soc., 136, 411–425, https://doi.org/10.1002/qj.538, 2010.

Hartmann, D. L., Hendon, H. H., and Houze, R. A.: Some implications of the mesoscale circulations in tropical cloud clusters for the large-scale dynamics of the tropics, J. Atmos. Sci., 41, 113–121, https://doi.org/10.1175/1520-0469(1984)041<0113:SIOTMC>2.0.CO;2, 1984.

Hartmann, D. L., Moy, L. A., and Fu, Q.: Radiative effects of tropical cloud systems, J. Atmos. Sci., 41, 81–90, https://doi.org/10.1175/1520-0469(1984)041<0081:REOTCS>2.0.CO;2, 1984.

Houze, R. A.: Cloud clusters and large-scale vertical motions in the tropics, J. Meteorol. Soc. Jpn., 60, 396–410, https://doi.org/10.2151/jmsj1965.60.1_396, 1982.

Ioffe, S. and Szegedy, C.: Batch normalization: Accelerating deep network training by reducing internal covariate shift, in: Proceedings of the 32nd International Conference on Machine Learning, Lille, France, 6–11 July 2015, 448–456, 2015.

Kidd, C., Huffman, G., Maggioni, V., Chambon, P., and Oki, R.: The Global Satellite Precipitation Constellation: Current status and future requirements, B. Am. Meteorol. Soc., 102, E1844–E1861, https://doi.org/10.1175/BAMS-D-20-0299.1, 2021a.

Kidd, C., Matsui, T., and Ringerud, S.: Precipitation retrievals from passive microwave cross-track sensors: The Precipitation Retrieval and Profiling Scheme, Remote Sens., 13, 947, https://doi.org/10.3390/rs13050947, 2021b.

Kidd, C., Matsui, T., Blackwell, W., Braun, S., Leslie, R., and Griffith, Z.: Precipitation estimation from the NASA TROPICS mission: Initial retrievals and validation, Remote Sens., 14, 2992, https://doi.org/10.3390/rs14132992, 2022.

https://doi.org/10.5194/egusphere-2026-4156
Preprint. Discussion started: 2 September 2026

Kidd, C., Matsui, T., Kummerow, C. D., and Randel, D. L.: Global precipitation estimates from cross-track passive microwave observations using a physically based retrieval scheme, J. Hydrometeorol., 17, 383–400, https://doi.org/10.1175/JHM-D-15-0051.1, 2016.

Kingma, D. P. and Ba, J.: Adam: A method for stochastic optimization, in: Proceedings of the 3rd International Conference on Learning Representations, San Diego, CA, USA, 7–9 May 2015, 2015.

Kummerow, C. D., Randel, D. L., Kulie, M., Wang, N.-Y., Ferraro, R., Munchak, S. J., and Petković, V.: The evolution of the Goddard Profiling Algorithm to a fully parametric scheme, J. Atmos. Ocean. Tech., 32, 2265–2280, https://doi.org/10.1175/JTECH-D-15-0039.1, 2015.

Lang, S. E. and Tao, W.-K.: The next-generation Goddard Convective–Stratiform Heating algorithm: New tropical and warm-season retrievals for GPM, J. Climate, 31, 1544–1601, 2018.

Li, X., and co-authors: Passive-microwave precipitation detection using convolutional neural networks, IEEE Geosci. Remote S., 18, 1–5, 2021.

Lin, M., Chen, Q., and Yan, S.: Network in network, arXiv [preprint], arXiv:1312.4400, 2013.

Loeb, N. G., Su, W., Doelling, D. R., Wong, T., Minnis, P., Thomas, S., and Miller, W. F.: Earth's top-of-atmosphere radiation budget, in: Reference Module in Earth Systems and Environmental Sciences, Elsevier, https://doi.org/10.1016/B978-0-12-409548-9.10367-7, 2016.

Loeb, N. G., Wielicki, B. A., Doelling, D. R., Smith, G. L., Keyes, D. F., Kato, S., and Wong, T.: Toward optimal closure of the Earth's top-of-atmosphere radiation budget, J. Climate, 22, 748–766, https://doi.org/10.1175/2008JCLI2637.1, 2009.

Mapes, B. E.: Water's two height scales: The moist adiabat and the radiative troposphere, Q. J. Roy. Meteorol. Soc., 127, 2353–2366, https://doi.org/10.1002/qj.49712757708, 2001.

Matsui, T., Tao, W.-K., Munchak, S. J., Huffman, G., and Grecu, M.: Satellite view of quasi-equilibrium states in tropical convection and precipitation microphysics, Geophys. Res. Lett., 42, https://doi.org/10.1002/2015GL063261, 2015.

Munchak, S. J., and co-authors: On-orbit calibration of the Tomorrow.io microwave sounders, ESS Open Archive [preprint], https://doi.org/10.22541/essoar.175250254.43121152/v1, 2025.

Nair, V. and Hinton, G. E.: Rectified linear units improve restricted Boltzmann machines, in: Proceedings of the 27th International Conference on Machine Learning, Haifa, Israel, 21–24 June 2010, 807–814, 2010.

https://doi.org/10.5194/egusphere-2026-4156
Preprint. Discussion started: 2 September 2026

Nesbitt, S. W., Zipser, E. J., and Cecil, D. J.: A census of precipitation features in the tropics using TRMM: Radar, ice scattering, and lightning observations, J. Climate, 13, 4087–4106, https://doi.org/10.1175/1520-0442(2000)013<4087:ACOPFI>2.0.CO;2, 2000.

Olson, W. S. and the GPM Combined Radar-Radiometer Algorithm Team: GPM Combined Radar-Radiometer Precipitation Algorithm Theoretical Basis Document, Version 7, NASA Goddard Space Flight Center, Greenbelt, MD, USA, available at: https://gpm.nasa.gov/sites/default/files/2023-01/Combined_algorithm_ATBD.V07_0.pdf (last access: 1 July 2026), 2022.

Paszke, A., Gross, S., Massa, F., Lerer, A., Bradbury, J., Chanan, G., Killeen, T., Lin, Z., Gimelshein, N., Antiga, L., Desmaison, A., Köpf, A., Yang, E., DeVito, Z., Raison, M., Tejani, A., Chilamkurthy, S., Steiner, B., Fang, L., Bai, J., and Chintala, S.: PyTorch: An imperative style, high-performance deep learning library, in: Advances in Neural Information Processing Systems 32 (NeurIPS 2019), Vancouver, BC, Canada, 8–14 December 2019, 8024–8035, 2019.

Pfreundschuh, S., Brown, P. J., Kummerow, C. D., Eriksson, P., and Norrestad, T.: GPROF-NN: A neural-network-based implementation of the Goddard Profiling Algorithm, Atmos. Meas. Tech., 15, 5033–5060, https://doi.org/10.5194/amt-15-5033-2022, 2022.

PyTorch Developers: AdaptiveAvgPool2d documentation, available at: https://pytorch.org/ (last access: 1 August 2026), 2025.

Riehl, H. and Malkus, J. S.: On the heat balance in the equatorial trough zone, Geophysica, 6, 503–538, 1958.

Sadeghi, M., Asanjan, A. A., Faridzad, M., Nguyen, P., Hsu, K., Sorooshian, S., and Braithwaite, D.: PERSIANN-CNN: Precipitation estimation from remotely sensed information using artificial neural networks–convolutional neural networks, J. Hydrometeorol., 20, 2273–2289, https://doi.org/10.1175/JHM-D-19-0110.1, 2019.

Sanò, P., Panegrossi, G., Casella, D., Marra, A. C., Di Paola, F., and Dietrich, S.: The Passive microwave Neural network Precipitation Retrieval algorithm for climate applications (PNPR-CLIM): Design and verification, Remote Sens., 10, 1122, https://doi.org/10.3390/rs10071122, 2018.

Satoh, S. and Noda, A.: Retrieval of latent heating profiles from TRMM radar data, 30th International Conference on Radar Meteorology, Munich, Germany, 19–24 July 2001, 6.3, 2001.

Schumacher, C., Houze, R. A., and Kraucunas, I.: The tropical dynamical response to latent heating estimates derived from the TRMM precipitation radar, J. Atmos. Sci., 61, 1341–1358, https://doi.org/10.1175/1520-0469(2004)061<1341:TTDRTL>2.0.CO;2, 2004.

https://doi.org/10.5194/egusphere-2026-4156
Preprint. Discussion started: 2 September 2026

Shige, S., Takayabu, Y. N., Tao, W.-K., and Johnson, D. E.: Spectral retrieval of latent-heating profiles from TRMM PR data. Part I: Development of a model-based algorithm, J. Appl. Meteorol., 43, 1095–1113, https://doi.org/10.1175/1520-0450(2004)043<1095:SROLHP>2.0.CO;2, 2004.

Srivastava, N., Hinton, G., Krizhevsky, A., Sutskever, I., and Salakhutdinov, R.: Dropout: A simple way to prevent neural networks from overfitting, J. Mach. Learn. Res., 15, 1929–1958, 2014.

Staelin, D. H. and Chen, F. W.: Precipitation observations near 54 and 183 GHz using the NOAA-15 satellite, IEEE T. Geosci. Remote, 38, 2322–2332, https://doi.org/10.1109/36.868889, 2000.

Stephens, G. L., Li, J.-L., Wild, M., Clayson, C. A., Loeb, N., Kato, S., L'Ecuyer, T., Stackhouse, P. W., Lebsock, M., and Andrews, T.: An update on Earth's energy balance in light of the latest global observations, Nat. Geosci., 5, 691–696, https://doi.org/10.1038/ngeo1580, 2012.

Surussavadee, C. and Staelin, D. H.: Global millimeter-wave precipitation retrievals trained with a cloud-resolving numerical weather prediction model. Part I: Retrieval design, IEEE T. Geosci. Remote, 46, 99–108, https://doi.org/10.1109/TGRS.2007.908302, 2008.

Tang, G., Long, D., Behrangi, A., Wang, C., and Hong, Y.: Exploring deep neural networks to retrieve rain and snow in high latitudes using multisensor and reanalysis data, Water Resour. Res., 54, 8253–8278, https://doi.org/10.1029/2018WR023830, 2018.

Tao, W.-K. and Lang, S.: Goddard Convective-Stratiform Heating (CSH) Algorithm, Global Precipitation Measurement (GPM) Algorithm Theoretical Basis Document (ATBD), NASA Goddard Space Flight Center, Greenbelt, MD, USA, available at: https://gpm.nasa.gov/sites/default/files/document_files/CSH_ATBD.pdf (last access: 1 July 2026), 2016.

Tao, W.-K., Iguchi, T., and Lang, S.: Expanding the Goddard CSH algorithm for GPM: New extratropical retrievals, J. Appl. Meteorol. Clim., 58, 921–946, https://doi.org/10.1175/JAMC-D-18-0215.1, 2019.

Tao, W.-K., Lang, S., Iguchi, T., and Song, Y.: Goddard latent heating retrieval algorithm for TRMM and GPM, J. Meteorol. Soc. Jpn., 100, 293–320, https://doi.org/10.2151/jmsj.2022-015, 2022.

Tao, W.-K., Lang, S., Simpson, J., and Adler, R.: Retrieval algorithms for estimating the vertical profiles of latent heat release: Their applications for TRMM, J. Meteorol. Soc. Jpn., 71, 685–700, 1993.

Tao, W.-K., Lang, S., Simpson, J., Olson, W. S., Johnson, D. E., Grecu, M., Yang, S., Shige, S., Takayabu, Y., Lau, W. K.-M., and Kummerow, C.: Retrieval of latent heating from TRMM

https://doi.org/10.5194/egusphere-2026-4156
Preprint. Discussion started: 2 September 2026

measurements, B. Am. Meteorol. Soc., 87, 1555–1572, https://doi.org/10.1175/BAMS-87-11-1555, 2006.

Tao, W.-K., Lang, S., Zeng, X., Shige, S., and Takayabu, Y.: Relating convective and stratiform rain to latent heating, J. Climate, 23, 1874–1893, https://doi.org/10.1175/2009JCLI3278.1, 2010.

Webster, P. J.: Response of the tropical atmosphere to local steady forcing, Mon. Weather Rev., 100, 518–541, https://doi.org/10.1175/1520-0493(1972)100<0518:ROTTAT>2.3.CO;2, 1972.

Wielicki, B. A., Barkstrom, B. R., Harrison, E. F., Lee III, R. B., Smith, G. L., and Cooper, J. E.: Clouds and the Earth's Radiant Energy System (CERES): An Earth Observing System experiment, B. Am. Meteorol. Soc., 77, 853–868, https://doi.org/10.1175/1520-0477(1996)077<0853:CATERE>2.0.CO;2, 1996.

Yanai, M., Esbensen, S., and Chu, J.-H.: Determination of bulk properties of tropical cloud clusters from large-scale heat and moisture budgets, J. Atmos. Sci., 30, 611–627, https://doi.org/10.1175/1520-0469(1973)030<0611:DOBPOT>2.0.CO;2, 1973.

Yang, J. X., Lee, Y.-K., Grassotti, C., Garrett, K., Liu, Q., Blackwell, W., Leslie, R. V., Greenwald, T., Bennartz, R., and Braun, S.: Atmospheric humidity and temperature sounding from the CubeSat TROPICS mission: Early performance evaluation with MiRS, Remote Sens. Environ., 287, 113479, https://doi.org/10.1016/j.rse.2023.113479, 2023.

Yang, S. and Smith, E. A.: Moisture budget analysis of TOGA COARE area using SSM/I-retrieved latent heating and large-scale Q2 estimates, J. Atmos. Ocean. Tech., 16, 633–655, https://doi.org/10.1175/1520-0426(1999)016<0633:MBAOTC>2.0.CO;2, 1999.

Zhu, X. X., Tuia, D., Mou, L., Xia, G.-S., Zhang, L., Xu, F., and Fraundorfer, F.: Deep learning in remote sensing: A comprehensive review and list of resources, IEEE Geosci. Remote S., 5, 8–36, https://doi.org/10.1109/MGRS.2017.2762307, 2017.